University of South Bohemia

Faculty of Science

Optimization of Supercontinuum Generation in the UV through Near IR Spectral Region

Bachelor Thesis

Nikola Horová

Supervisor of the bachelor thesis: Mgr. Marcel Fuciman, Ph.D.

České Budějovice 2017

This thesis should be cited as:

Horová, N., 2017: Optimization of Supercontinuum Generation in the UV through Near IR Spectral Region. [Optimalozace generace superkontinua v UV až blízké IR oblasti., Bc. Thesis, in English]-41 p., Faculty of Science, University of South Bohemia, České Budějovice, Czech Republic.

Annotation:

Supercontinuum generation occurs when a laser pulse with high intensity passes through an optical medium. The white light is a combination of several nonlinear effects and thus depends on the various parametres. The main task of this bachelor thesis is to find parametres (a focal length, energy of pulse, a diameter of an aperture) for the white light generation in the UV through near IR region in 2-3mm thin crystal plates of sapphire, quartz and YAP.

Keywords: supercontinuum generation, nonlinear optics, focal length, spectra, femtosecond laser pulses

Declaration [in Czech]

Prohlašuji, že svoji bakalářskou práci jsem vypracovala samostatně pouze s použitím pramenů a literatury uvedených v seznamu citované literatury.

Prohlašuji, že v souladu s §47b zákona č. 111/1998 Sb. v platném znění souhlasím se zveřejněním své bakalářské práce, a to v nezkrácené podobě elektronickou cestou ve veřejně přístupné části databáze STAG provozované Jihočeskou univerzitou v Českých Budějovicích na jejích internetových stránkách, a to se zachováním mého autorského práva k odevzdanému textu této kvalifikační práce. Souhlasím dále s tím, aby toutéž elektronickou cestou byly v souladu s uvedeným ustanovením zákona č. 111/1998 Sb. zveřejněny posudky školitele a oponentů práce i záznam o průběhu a výsledky obhajoby kvalifikační práce. Rovněž souhlasím s porovnáním textu mé kvalifikační práce s databází kvalifikačních prací Theses.cz provozovanou Národním registrem vysokoškolských kvalifikačních prací a systémem na odhalování plagiátů.

V ..... datum ..... podpis autora

Acknowledgements

My deep gratitude goes first to my supervisor Mgr. Marcel Fuciman, Ph.D. for all support, patience and knowledges.

I would also like to say thank you to my Mum, Dad, Sister and whole family for being always here for me.

Last but not the least, there are two persons who always help me with problems I have. Thank you, David and Ivča for being a part of my life.

Contents

1 Introduction

Stimulated emission of radiation and a principle of laser were known since the beginning of the 20^{th} century. However, due to technical complications the first working example was constructed in 1960 by Maiman and collective. It allowed to generate higher intensities of light and therefore helped to discover a new class of optical effects. These include nonlinearities which are important for my study.

In general, the dependence of a vector of electric intensity $\mathbf{E}$ and a vector of polarization $\mathbf{P}$ is not linear. A consequence of this relation is dispersion - the refractive index and the velocity of propagating light wave change with electric intensity $\mathbf{E}$. Moreover, the superposition theorem does not hold and the wave frequency is influenced by a material which it passes through.

Differences between the linear and nonlinear dependence $\mathbf{E}(\mathbf{P})$ lead to various effects, e.g. second-harmonic generation, phase matching, parametric up-conversion, optical parametric amplification or the white light generation (see section 2.2). The mathematical description of mentioned phenomena is rather difficult and is not a part of this thesis.

Ten years after the discovery of the first working laser, Shapiro and Alfano reported an effect called spectral broadening, which led to white light generation [8]. They explained it through self-phase modulation and four-wave mixing. However, this was not sufficient and since then many attempts have been introduced to describe the generation of the white light. Nowadays, the pulse-self steeping leading to optical shock wave formation is taken as the main process of the supercontinuum generation, see e.g. [1].

In the laboratory of optical spectroscopy where this work has been done, the transient spectroscopy using the pump-probe method is measured.

The spectra of the white light continuum are generated by crystal plates made from sapphire with thickness about 2-3 mm. The reason is an effort to have supercontinuum with as small group velocity dispersion as possible. The main aim of this thesis is to examine possibilities for wider spectral range of measuring apparatus, mainly in the way of enhancing the supercontinuum generation. For example, in article [10], the thicker plates (5mm) are used. They generate beautiful broadband spectra but with significant group velocity dispersion.

2 | Nonlinear Optics

In this chapter, we consider the basic relations of description of nonlinear phenomena. With their help, step by step, we reach our main target- supercontinuum generation which is a combination of these effects. The most used literature is a book *Nonlinear optics* written by Boyd [1] and from this reason, its reference will not be written at the end of each paragraph.

2.1 Basic equations of nonlinear optics

To better understand the meaning of the optical nonlinearity, we have to consider how polarization $P(t)$ of a material depends on an applied optical field $E(t)$ [1, 4]. In a linear and isotropic dielectric medium, the polarization is directly proportional to the electric field

$$P(t) = \varepsilon_0 \chi E(t), \tag{2.1}$$

where ε_0 is the permittivity of vacuum and χ is the linear susceptibility. We can generalize the previous equation by expressing polarization $P(t)$ by power series in the electric field $E(t)$

$$P(t) = \varepsilon_0[\chi^{(1)}E(t) + \chi^{(2)}E^2(t) + \chi^{(3)}E^3(t) + \cdots] \equiv P^{(1)}(t) + P^{(2)}(t) + P^{(3)}(t) + \cdots, \tag{2.2}$$

where $\chi^{(n)}, n \in \mathbb{N}$ are nonlinear optical susceptibilities of the n-th order.

In (2.1) are $P(t)$ and $E(t)$ scalars. It is the consequence of having linear and isotropic dielectric medium. But in general, these quantities are vectors and $\boldsymbol{\chi}^{(n)}, n \in \mathbb{N}$ become tensors. We also assumed no energy losses and no dispersion.

Further, we consider only the second term in the Eq. (2.2)

$$P^{(2)}(t) = \varepsilon_0 \chi^{(2)} E^2(t). \tag{2.3}$$

Materials characterized by this relation are referred as second-order nonlinear optical media [2].

We move to investigating the interaction of two harmonic waves

$$E_1(t) = e^{-i\omega_1 t},$$
$$E_2(t) = e^{-i\omega_2 t}.$$

The total wave $E(t)$ is given by superposition of these particular waves

$$E(t) = E_1(t) + E_2(t)$$

A substitution to Eq. (2.3) yields

$$\begin{aligned} P^{(2)}(t) = \varepsilon_0 \chi^{(2)} [E_1^2(t) e^{-2i\omega_1 t} + E_2^2(t) e^{-2i\omega_2 t} + 2E_1(t)E_2(t) e^{-i(\omega_1+\omega_2)t} \\ + 2E_1(t)E_2{}^*(t) e^{-i(\omega_1-\omega_2)t} + c.c.] + 2\varepsilon_0 \chi^{(2)} [E_1 E_1{}^* + E_2 E_2{}^*], \end{aligned}$$

where *c.c.* denotes a complex conjugation. Using the elementary trigonometric relations

$$\begin{aligned} \cos\alpha \cos\beta &= \frac{1}{2}(\cos(\alpha+\beta) + \cos(\alpha-\beta)), \\ \cos^2\alpha &= \frac{1}{2}(1 - \cos 2\alpha), \end{aligned}$$

we can write the polarization in separate terms belonging to different frequencies

$$\begin{aligned} P_{2\omega_1} &= \varepsilon_0 \chi^{(2)} E_1^2 && \text{(SHG)}, \\ P_{2\omega_2} &= \varepsilon_0 \chi^{(2)} E_2^2 && \text{(SHG)}, \\ P_{\omega_1+\omega_2} &= 2\varepsilon_0 \chi^{(2)} E_1 E_2 && \text{(SFG)}, \\ P_{\omega_1-\omega_2} &= 2\varepsilon_0 \chi^{(2)} E_1 E_2{}^* && \text{(DFG)}, \\ P_0 &= 2\varepsilon_0 \chi^{(2)} (E_1 E_1{}^* + E_2 E_2{}^*) && \text{(OR)}. \end{aligned} \tag{2.4}$$

The shortcuts in the brackets denotes names of effects which we want to describe. They are namely *second harmonic generation* (SHG), *sum-frequency generation* (SFG), *difference-frequency generation* (DFG) and *optical rectification* (OR). In the following text, the shortcuts are occasionally used for brevity.

2.2 Important processes and phenomena

In the previous section, we generalized the Eq. (2.1) for polarization by power series (2.2) in an applied field E. We also considered only the second order term, which yielded to the Eq. (2.3). As already mentioned above, this relation describes the second-order nonlinear media and it is linked with various processes. However, if we have a medium (crystal) with a central symmetry, the second order polarization $P^{(2)}$ is identically zero. The lowest nonlinear contribution is given by $P^{(3)}$, while the fourth and higher order terms can be again neglected. These media are usually called the *Kerr's media* (see Section 2.2.7) and they are connected with phenomenons like the third harmonic generation (THG) and the self-action effects (see Section 2.2.8). Since the Kerr's media and related phenomena are the most important for our work, we approach to more precise description of them.

2.2.1 Sum-frequency and difference-frequency generation

As we introduced in the Eq. (2.4), the sum-frequency generation is described by the term

$$P_{\omega_1+\omega_2} = 2\varepsilon_0\chi^{(2)}E_1E_2.$$

The waves E_1 and E_2, proceeding through a second-order optical medium (see also fig. 2.1), sum to one wave E with frequency

$$\omega_3 = \omega_1 + \omega_2,$$

A practical application of this equation is tuning the wavelength of lasers. For example, if we choose one of the input waves as the output of a laser with a frequency in the visible region, which is fixed, and the second one as the output of a laser with a frequency again in the visible region, which is tunable, then we can produce a tunable radiation in the ultraviolet region.

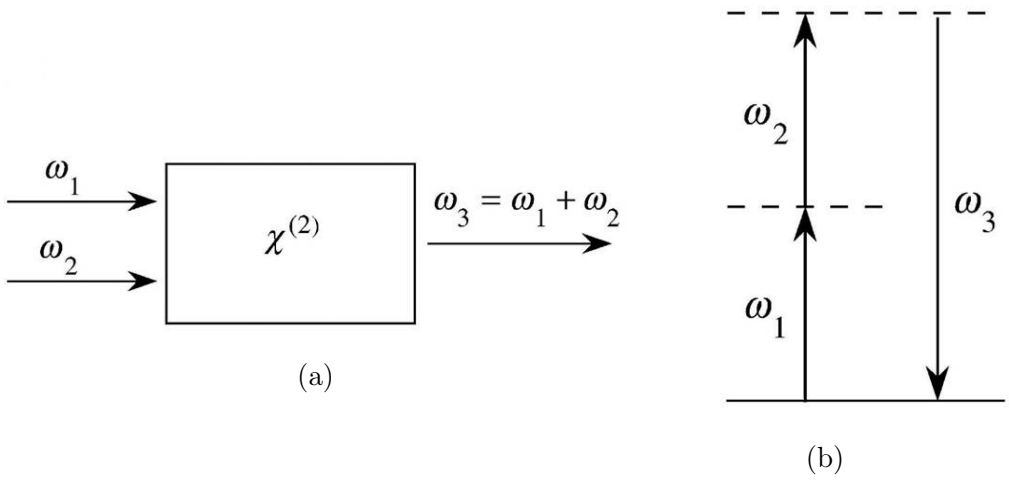

Figure 2.1: The description of the sum-frequency generation. This figure is taken from [1]
(a) Simplified scheme.
(b) Energy-level diagram

According to (2.4), difference-frequency generation is determined by the condition

$$P_{\omega_1-\omega_2} = 2\varepsilon_0\chi^{(2)}E_1E_2^*.$$

It is analogous to the sum-frequency generation, except that in the case of difference-frequency generation, the frequency of the generated wave is the difference of the two input waves. We use it to produce a tunable infrared radiation.

The main difference between SFG and DFG is illustrated the figure 2.2. Consider two waves with frequencies $\omega_1 > \omega_2$ proceeding the second-order nonlinear medium. We assume that ω_1 is sufficiently high to excite atoms of the medium and ω_2 was chosen to be

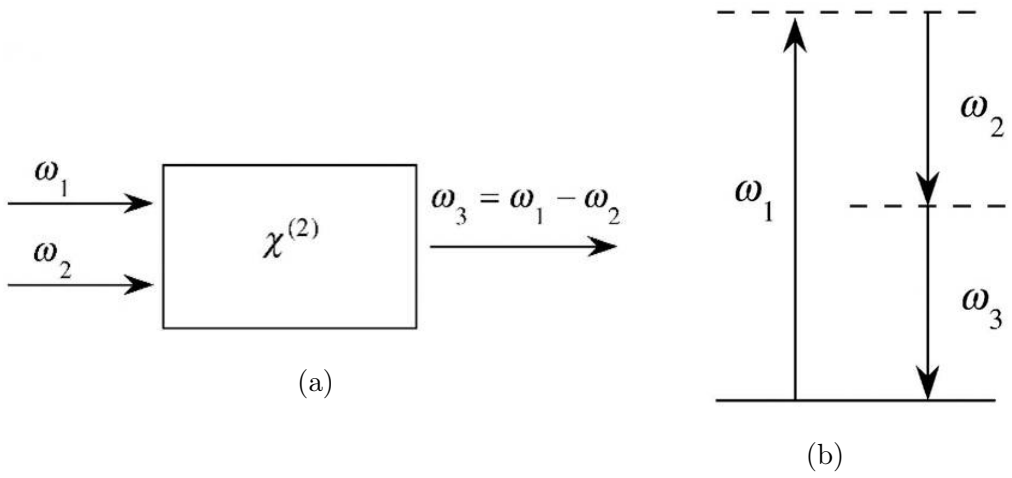

Figure 2.2: The decription of the difference-frequency generation. This figure is taken from [1]
(a) Simplified scheme.
(a) Energy-level diagram.

$\omega_2 = \omega_1 - \omega_3$. An excited atom moves to lower energy level by interaction with photon of frequency ω_2 emitting a photon of the same frequency ω_2. Because of the energy conservation, it returns to its ground state emitting photon of frequency ω_3 (see fig. 2.2 **(b)**).

The part **(b)** shows a photon energy-level diagram. Energy conservation implies that every photon with the frequency ω_3 created by difference frequency generation. Usually, we call SFG as up-conversion and DFG as down-conversion process. The up and down attribute corresponds to the "direction" of the frequency change. Up-conversion is another special case of sum frequency generation as well as SHG. Up-conversion materials can be used to visually detect infrared radiation or to up-converse lasers which, because of up-conversion process, have larger output power[2].

A special case of sum-frequency and difference-frequency generation is optical rectification. A condition $\omega_1 = \omega_2$ has to be satisfied in the Eq. 2.4. Then $\omega_3 = 0$ and DC signal is generated. Optical rectification is based on the inverse process to electro-optic effect and it is one of the main mechanisms of generation of terahertz radiation in the laser optics [5].

2.2.2 Optical parametric oscillator

When we described the process of the difference-frequency generation, we mentioned stimulate emission with frequencies ω_2 and ω_3. If we put a nonlinear medium, e.g. crystal, used in DFG process into an optical resonator, we can achieve that ω_2 and ω_3 will be very high (both or at least one of them). Frequency $\omega_1 = \omega_2 + \omega_3$ is usually called

the pump frequency. Frequency ω_2 is called the signal frequency and ω_3 is known as idler. Such a device is tunable because we can satisfy the condition $\omega_1 = \omega_2 + \omega_3$ for some frequencies ω_3, $\omega_2 < \omega_1$ and its name is optical parametric oscillator[1, 2].

2.2.3 Second-harmonic generation

In the linear approximation, optical properties of materials depend only on the light frequency. This frequency is constant as the light passes through the material. However, optical properties of real materials are, in general, functions of frequency and light intensity (even other parameters). Moreover, the frequency is not constant yet, so we have to find out the influence of hight light intensities on the material. Further, we deal with nonlinear quadratic dependence according to Eq. (2.3)[1, 5].

Let us consider a laser beam whose electric field is

$$\tilde{E}(t) = Ee^{-i\omega t} + c.c., \tag{2.5}$$

where E is a constant amplitude. Substituting to Eq. (2.3) we get explicitly

$$\tilde{P}(t) = 2\varepsilon_0\chi^{(2)}EE^* + (\varepsilon_0\chi^{(2)}E^2e^{-i2\omega t} + c.c.). \tag{2.6}$$

The first term is contribution of the second-order polarization at zero frequency and the second term is a contribution at frequency 2ω. The latter term is responsible for the generation of radiation with the second harmonic frequency 2ω. The second differentiation of the first term with respect to t gives zero, so it can not lead to the second harmonic generation. But it leads to a process known as optical rectification, which we mentioned before.

Practically, the effect is used to change the frequency of radiation. In the visual region of spectrum, this effect causes a change of outgoing beam color, so we can transform radiation e.g. from the infrared region into the visible region. The process is, however, more difficult as we described. Additional conditions have to be satisfied. We discuss them more precisely in the section 2.2.6.[5]

2.2.4 Third-harmonic generation

Light generation with a tripled frequency to the initial one is called *third-harmonic generation*. In this process, three photons (e.g. from the same laser beam) are annihilated while only one at corresponding frequency is created. The polarization in Kerr's media can be taken as

$$P(t) = P^{(1)}(t) + P^{(3)}(t) = \varepsilon_0[\chi^{(1)}E(t) + \chi^{(3)}E^3(t)], \tag{2.7}$$

where $P^{(1)}(t)$ is the linear and $P^{(3)}(t)$ is the third-order nonlinear polarization and $\chi^{(1)}$ is the linear and $\chi^{(3)}$ is the third-order nonlinear susceptibility.

In general, related effects are observable only at higher intensities of light than are needed in the case of the second-harmonic generation, except media with the central symmetry. In noncentrosymmetric crystals, the frequency tripling, phase-matched by anisotropic crystals (see Section 2.2.6), is implemented through cascaded second-order nonlinear-optical effects [7, 5].

2.2.5 Four-wave mixing

Four-wave mixing is a generalized case of the harmonic generation with a cubic nonlinearity $\chi^{(3)}$ [5]. Consider an interaction of three traveling waves $E_1(t)$, $E_2(t)$ and $E_3(t)$ with frequencies ω_1, ω_2 and ω_3 . This situation is analogous to the process with two traveling waves $E_1(t)$ and $E_2(t)$ in the second-order optical medium which we previously described (see Section 2.1). However, when we add the third wave with the frequency ω_3, we get 44 different possible frequencies. For example for positive frequencies

$$\begin{gathered} 3\omega_1, 3\omega_2, 3\omega_3, \\ (\omega_1+\omega_2+\omega_3), (\omega_1+\omega_2-\omega_3), (\omega_1+\omega_3-\omega_2), (\omega_2+\omega_3-\omega_1), \\ (2\omega_1 \pm \omega_2), (2\omega_1 \pm \omega_3), (2\omega_2 \pm \omega_3), (2\omega_2 \pm \omega_1), (2\omega_3 \pm \omega_1), (2\omega_3 \pm \omega_2), \\ \omega_1, \omega_2, \omega_3. \end{gathered} \tag{2.8}$$

The first three expressions describe the third-harmonic generation (THG). The *possible mixing processes* are expressed in the second row. Other expressions in brackets describe the *sum-frequency generation* (SFG) and the *diference-frequency generation* (DFG).

2.2.6 Phase-matching

When we want to reach high efficiency of radiation frequency changes, we need to have a same velocity for waves located in a medium. It is often not easy to satisfy, since in the most nonlinear optical media, the refractive index is an increasing function of frequency $n = n(f)$. In anisotropic uniaxial crystals, on the other hand, it is possible. [5]

As the incident light passes through an anisotropic uniaxial crystal, this incident light is split into two polarized rays. One of them is known as the *ordinary ray* (o-ray) and the other one as the extraordinary ray (e-ray). The first ray follows Snell's law and has polarization in a direction perpendicular to the optical axis. The refractive index and the propagating velocity do not depend on the angle of propagating light. We can describe this dependence by a circle (see figure 2.3 (a)). In contrast, the second ray does not follow Snell's law and has polarization in the direction of the optical axis of the medium. [6].

The value of the refractive index is same for both rays (e-ray, o-ray) only if they pass the medium in the direction of the optical axis. In other directions for extraordinary ray,

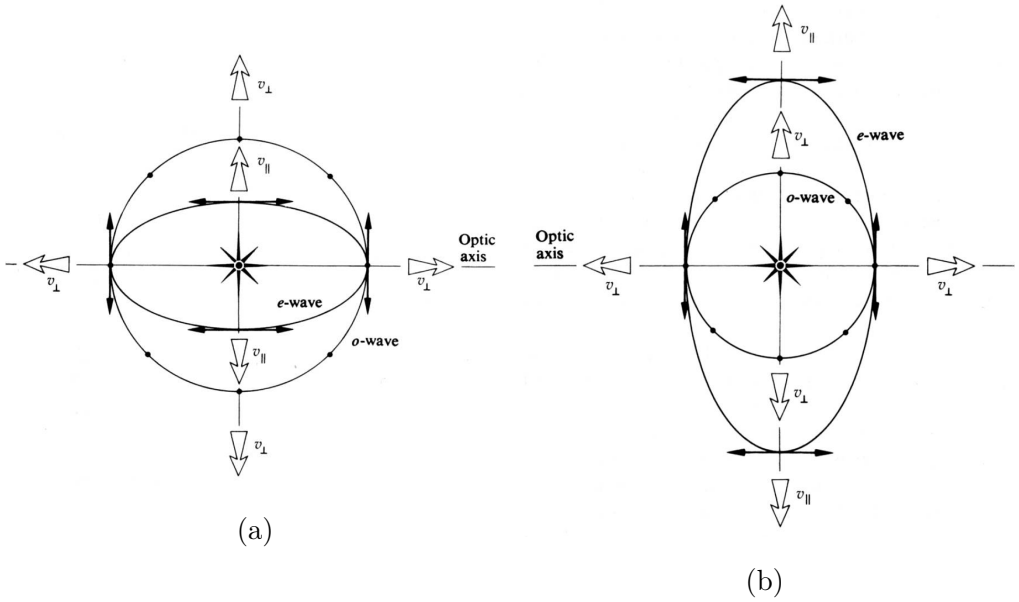

Figure 2.3: Propagation of e-ray and o-ray in an anisotropic uniaxial crystal.
(a) Positive crystal. **(b)** Negative crystal.
This figure is taken from the book Optics by Eugene Hecht.

the value of the refractive index is lower (a negative crystal) or higher (a positive crystal) than in the previous case. We can describe this dependence by an ellipse. See Fig. 3. [5]

If we are lucky enough to choose the best combination of ordinary ray (the pump wave) and extraordinary ray (the second harmonic), we may reach a point where the both rays will propagate with the same velocity long enough to make the energy trasformation (between the pump wave and the second harmonic) effective. This phenomenon is called *phase-matching* and its advantage is in possibility to repeat this process to generate even harmonic frequencies (2ω, 4ω, ...).However, the phase-matching condition

$$\Delta k = 0 \tag{2.9}$$

where k is the wave vector, has to be satisfied This condition is often difficult to achieve because of an effect known as normal dispersion: $n = n(f)$, where n is the refractive index. [5].

For example, if we have $\omega_3 = \omega_1 + \omega_2$ (SFG), we get the wavevector mismatch

$$\Delta k = k_1 + k_2 - k_3. \tag{2.10}$$

Since we are interested in the condition for perfect phase-matching with collinear beams, we use Eq. (2.9) leads to

$$\frac{n_3\omega_3}{c} = \frac{n_1\omega_1}{c} + \frac{n_2\omega_2}{c}. \tag{2.11}$$

where c is the wave velocity. The condition for the second harmonic generation with $\omega_1 = \omega_2$ and $\omega_3 = 2\omega_1$ requires

$$n(\omega_1) = n(2\omega_1). \tag{2.12}$$

We can see that $n(\omega)$ can not increase monotonically with ω. This dependence is more complicated.[5]

One of the most common procedure to acheieve the phase-matching condition (2.9) is the use of birefringence in crystals. In birefringent crystals, the wave with highest frequency $\omega_3 = \omega_1 + \omega_2$ is polarized in the direction that gives it the lower of two possible refractive indices (Boyd, page 81). A negative uniaxial crystal with n_e as the lower refractive index is shown in Figure 2.4. Not all crystals display birefringence (see Table 2.1). In 1965, Midwinter and Warner defined two types of phase matching in crystals. Two lower-frequency waves with the same polarization belong to the type I and two lower frequency waves with orthogonal polarization belong to the type II.[2]

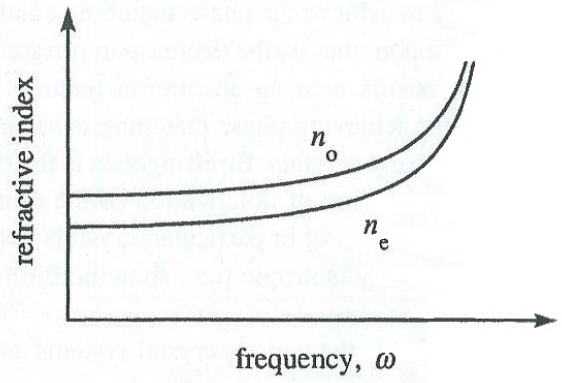

Figure 2.4: Dispersion in a negative uniaxial crystal. For a positive uniaxial crystal n_e and n_o indices are swapped. This figure is taken from [1]

Table 2.1: Optical classification of crystal systems

System	***Linear Opt. Classification - properties***
Triclinic, monoclinic, orthorhombic	Biaxial - show birefringence
Trigonal, tetragonal, hexagonal	Uniaxial - show birefringence
Cubic	Isotropic- no birefringence, no phase-matching

In practice, we use two methods to reach phase-matching in crystals: *angle tuning* and *temperature tuning*. The first one is based on dependence of the angular orientation of the crystal on the propagation direction of the incident light. The second one is based on the temperature dependence of refractive indices.[1]

In Figure 2.5, we can see differences among an ideally phase-matched crystal, a quasi phase-matched crystal and non-phase-matched crystal. Quasi phase-matching is another method for energy transformation. The advantage consists in using this method in the isotropic materials.

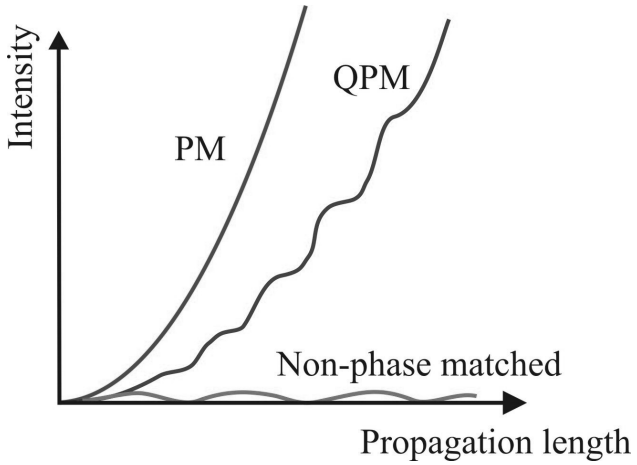

Figure 2.5: Phase-matching. The curve PM is perfect phase-matched. The curve QPM is quasi-phase-matched. This figure is taken from www.hcphotonics.com.

Many phase-sensitive nonlinear processes, such as SFG, DFG, parametric oscillation and four-wave mixing, require phase matching to be efficient. However, to make these effects in crystals possible, we have to assume that the phase-matching condition depends on a length of used crystals. We recognize two possibilities: The first one is already familiar to us. The wave vector k satisfies (2.9). It implies the linear dependence between the crystal length and the amplitude of the output wave. The second case includes a limit $\Delta k \to 0$ and the possibility that the wave at the econd harmonic frequency is still generated. Then, the dependence between the crystal length and the amplitude of the outgoing wave is described by a sinus function. For increasing Δk, we have to use shorter and shorter crystal length to satisfy the phase-matching condition.

2.2.7 Electrooptic effects

Static electric field applied on an isotropic optical medium can cause this medium to become anisotropic. The refractive index of the material changes with the strength of the applied field. In some materials, this dependence is linear and it is called the linear *electrooptic effect* or *Pockels effect*. However, in some materials, the change in the refractive index depends quadratically on the field strength. This quadratic dependence of the refractive index is known as the *quadratic electrooptic effect* or *Kerr electrooptic effect*. The linear electrooptic effect can occur only in noncentrosymetric materials.[1, 6]

Crystals are the most common anisotropic materials. Without an electric field, these crystals are uniaxial. The refractive index is in a direction of the propagating light. Hence, these crystals display no birefringence. On the other hand, if the electric field is applied in the direction of the crystal optical axis, the crystal becomes biaxial and displays the birefringence.[3]

The main use of the Pockels effect is in a device called the Pockels cell, which is used

as an electrooptic light modulator or as a Q-switch in an optical resonator. It serves to stop a generation of laser pulses for a specified time which is used for Q-switching of the open resonator. The principle of Q-switching is in a change of the resonator losses. Usually, the Pockels cell is placed between two crossed polarizators (half-wave) or between one polarizator and a reflective mirror (quarter wave). At the begining of the Q-switching process, one of the resonator mirrors is out of service because of the closed Q-switch. The resonator losses are huge and the generation of laser pulses is impossible. On the other hand, the population inversion increases (the state in which more atoms or molecules are in higher excited energy states than in lower unexcited energy states). Then, in a specified time (of the highest inversion), the Q-switch is opened. The the resonator losses are minimized and the short giant puls is generated.[3]

Anologous to the Pockels cell is the Kerr cell which uses the Kerr effect. This cell quickly modulates the light but a disadvantage is a large amount of energy needed for its function.

2.2.8 Self-action Effects

An effect of a light beam passing through a nonlinear medium modifying its own propagation is called *the self-action effect*. Generally, it is based on the Kerr effect [1, 5]. In the following we shortly describe just several particular phenomena belonging to this class.

A *self-focusing effect* is the result of a dependence of a refractive index on the electric field intensity **E**. If the refractive index is an increasing function of the intensity **E**, the light beam modifies the optical properties of a material in a such way[1] that it acts as a positive lens. Therefore, the rays approach to each other, as it is illustrated in Figure 2.6. [5]

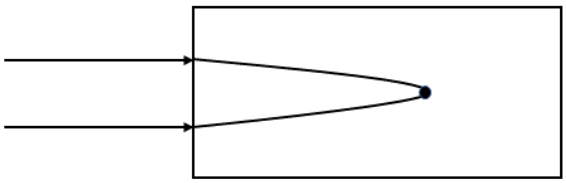

Figure 2.6: Self-focusing.

The opposite effect to self-focusing is a *self-defocusing effect*. Now, the refractive index decreases with increasing intensity **E**.The light beam has for that reason tendency to defocus. The situation is pictured in the figure 2.7

Diffraction plays a important role in an effect named *self-trapping of light*. It is the balance between the self-focusing and the diffraction what makes the propagating light beam to have a constant diameter as it passes through a material. For illustration see the figure 2.8.

The intensity of a laser beam can be varied in time. The impact is that the refractive index has almost the same functional dependence on time as the intensity of the laser beam

[1]It is related mainly to different beam intensities in the center than at the edges.

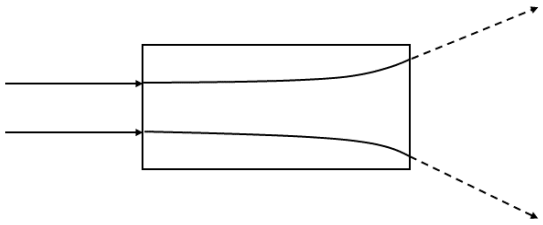

Figure 2.7: Self-defocusing.

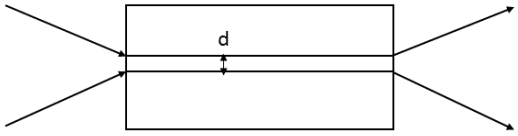

Figure 2.8: Self-trapping.

$\mathbf{E} = \mathbf{E}(t)$. We talk about *self-phase modulation*. This modulation of the refractive index produces a phase shift in pulses. The front of the pulse is shifted to lower frequencies (red-shift), while the back of the pulse is shifted to higher frequencies (blue-shift). For ultra-short pulses, this effect leads to significant spectrum-broadening.[6]

For intense very short broadband pulses, the intensity dependence on the refractive index, as was decribed in the Section 2.2.7, shows a deviation. Generally, the puls has a gaussian time evolution but after passing through a nonlinear medium, it displays a phenomenon called *self-steeping*. In the case of the positive refractive index n, the group velocity of the pulse peak slowed down more than the edges of the pulse and it leads to an increasing slope of the trailing part of the pulse. Then, an optical shock wave is formed when the trailing edge is infinitely steep.

Group velocity dispersion is an effect when the group velocity of light in an optical medium depends on the optical frequency or wavelength. It is responsible for broadening or compression of ultrashort pulses.

2.3 Supercontinuum Generation

A spectral broadening which appears in a profile of a short intense pulse propagating through a nonlinear optical medium is called *supercontinuum generation*. Many teories try to explain this phenomenon over the years. At present, a combination of various third-order nonlinear effects such as self-phase modulation and four-wave mixing leading to a spectral broadening of the pulse[6, 7] and the pulse self-steeping leading to shock-wave formation are the two most likely mechanisms of supercontinuum generation.[1]

3 | Materials and Methods

The white light generation requires high intensities of a laser beam to be generated. For this purpose, the laser system *The Spectra-Physics Spitfire®Ace^{TM}* providing 100 femtosecond pulses with a central wavelength around 800 nm and 1 kHz repetition rate was used. A setup of the apparatus used in our experiments is shown in the Figure 3.1 (a) and (b), respectively. It consists of a laser source, two mirrors, two variable filters, an aperture, a lens, a plate (quartz, sapphire and YAP[1]) and a spectrometer. In part (c) of the Figure 3.1 are pictured various distances, which were measured to get quantitative comparison of generated spectra. I denoted by f; s; L; α; z; l in order the following characteristics: the focal length; the equidistant distance between two spectra measured by one turn of a micrometer; the distance between the center of the used crystal and the point where the supercontinuum was measured; the angle between L and s; the distance between the center of a lens and the crystal plate; the distance between the crystal and the spectrometer.

The pulses from the laser system (1) were reflected by mirrors (2) on two metalic reflective neutral density filters (3) whose task was to reduce the intensity of radiation. Thanks to them, I was able to generate white light without damaging the plates and to observe the qualitative dependence of white light on energy of incoming pulses. The pulses continued through an iris aperture with adjustable diameter of the opening - a small device reducing the amount of radiation. The aperture plays an important role because it determines how collimated and homogeneous the rays are. If the aperture is small, the rays are highly collimated and the result is a sharp focus. In front of and behind the aperture, the input power P_1 and output power P_2 of the laser beam were measured by *Coherent®FieldMax II-TOP Laser Power and Energy Meter* with *OP-2 IR and OP-2 VIS sensors*. Then, the collimated rays passed through the converging lens, where they were focused, and continued to one of the three plates (quartz, sapphire or YAP). These plates were used as the medium for the white light generation. Their thickness was only 2 mm to minimize group velocity dispersion. After that, the white light continuum continued through one of *Longpass/Shortpass dichronic* filters to a *Sol 1.7 TE Cooled Linear InGaAs Array Spectrometer* by B&W Tek with wavelength range from 900 to 1700 nm or to a *USB2000+UV-VIS* by *OceanOptics*

[1] A shortcut for Yttrium Aluminum Perovskite.

with wavelength range from 190 to 1100 nm. Longpass filter used in this experiment served to transmit light of wavelength higher than 825 nm, other wavelengths were reduced. So, it serves as a filtration of the pump to prevent a damage of the spectrometer. The shortpass filter had the similar function. It reduced values under 780 nm and served to get only the spectra in the visible region. After that, the white light continuum entered a spectrometer and for various parameters (focal length, power, aperture diameter...) its spectra were measured (see Chapter 4).

When the crystal YAP was used as the medium, two qualitatively different continuum spectra were generated, depending on relative position with respect to the lens focus. These spectra are shown, e.g. in Figure 4.5. I named them YAP orange (Y_o) and YAP green (Y_g) because of their appearance.

The measurements of the distance between the center of the used crystal and the point where the supercontinuum was measured L, the distance between the crystal and the spectrometer l and the distance between the center of a lens and the crystal plate z were taken by a meter with a measurement error ± 1 mm. The distance s was obtained by a micrometer with a measurement error equal to ± 0.01 mm. This error is also characteristic for the diameter of the iris aperture. The focal length tolerance was given by the seller as $\pm 1\%$. The values of cut-off and cut-on were read from the graphs of spectra. Cut-on is a wavelength at which the transmission increases to 50% throughput in a longpass filter. Cut-off is a wavelength at which the transmission decreases to 50% throughput in a shortpass filter.

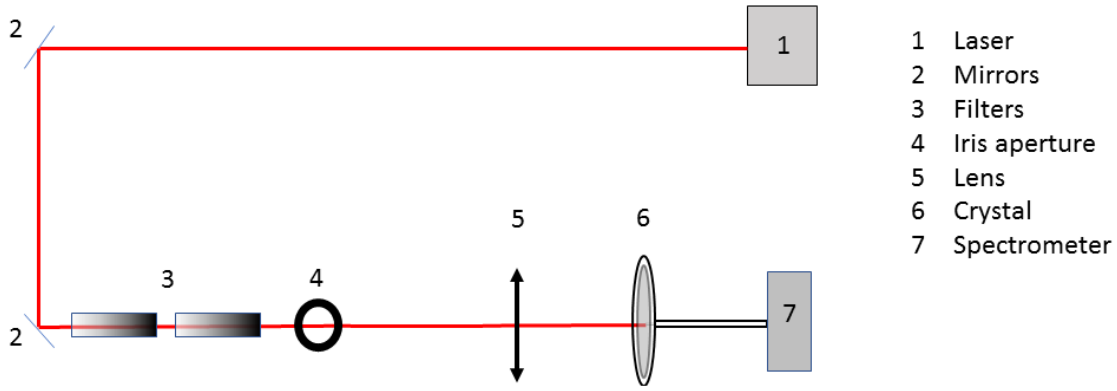

(a)

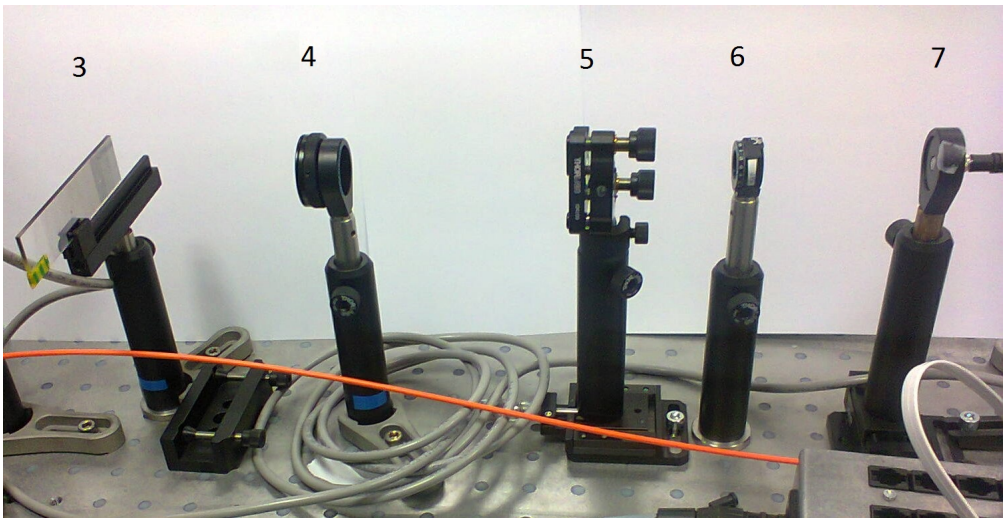

(b)

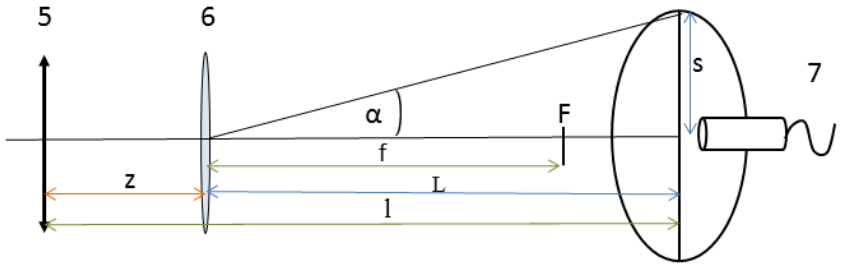

(c)

Figure 3.1: **(a)** An experimental setup - scheme. **(b)** Our setup - photography. **(c)** The description of all paremeters used in this setup

.

3.1 Quantitative description of supercontinuum spectra

Quantitative comparison of supercontinuum spectra is not straightforward as it may seem. Appropriate physical entities have to be chosen for description. We tried to figure out one possible way.

Initially, it is necessary to calculate the overall intensity of WL by integrating of a spectrum. The graph of a spectrum generated on sapphire is shown in Figure 3.2. The whole light intensity area I can be expressed as

$$I = \sum I_i. \tag{3.1}$$

The white light intensity I is a function of energy in a pulse P, the distance between the plate and spectrometer L and the quantity of pulses N (the number of pulses integrated by spectrometer). The intensity of light is indirectly proportional to the square of distance L from the source ($I_i = I_0/L^2$) and increases with increasing energy P and number of integrated pulses N ($I_i = I_0PN$). Then, the standardized light intensity is given by

$$I_n = \frac{L^2 \sum I_i}{PN}. \tag{3.2}$$

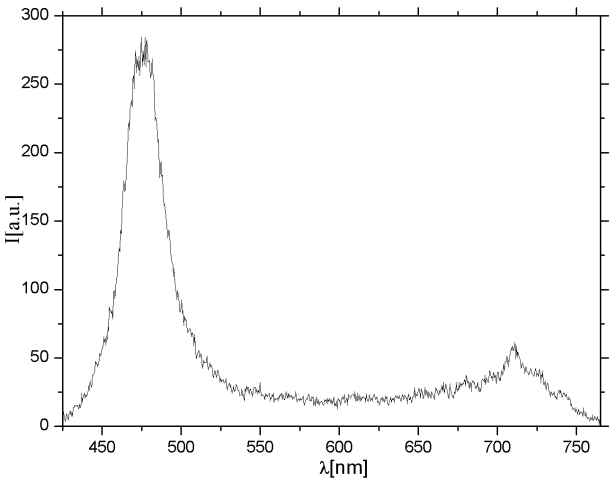

Figure 3.2: A white light spectrum generated on a sapphire plate

The next comparison of the white light continuum spectra is by its angular dependence. Supercontinuum spectra have not the same profiles in the various directions. The angle α between L and s is given by

$$\alpha = \arctan(s/L). \tag{3.3}$$

as is shown in Figure 3.1 part(c).

4 Spectra

In this chapter, the various graphs of the supercontinuum spectra generated in quartz, sapphire and YAP are shown. Here, they are compared in four various ways and separated into the visible and the infrared region. The first comparison takes only one crystal and compares its spectra for all focal lengths ($f = 75, 100, 150, 200, 250$ and 300 mm). In the second one all three crystal plates are taken for the same focal length and then their white light spectra are compared. In the third way, the differences between measured and standardized spectra are shown. Finally, only the best spectra from the previous comparisons are taken and their angular dependence is shown. In the last section of this chapter, the examples of spectra with wrong parameters are shown.

4.1 Visible spectral region

4.1.1 Spectra of quartz, sapphire and YAP for various focal lengths

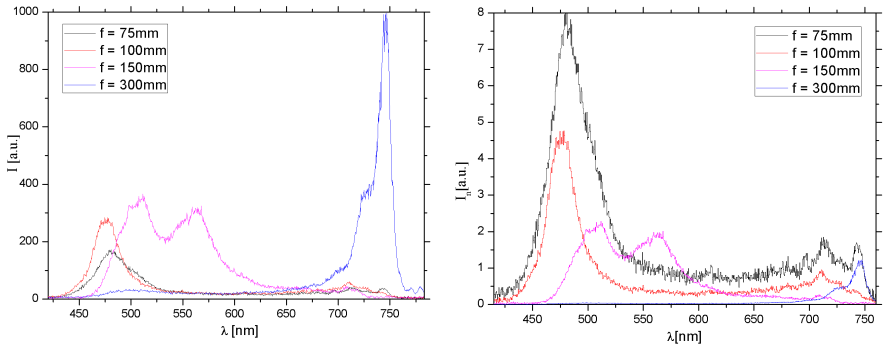

(a) (b)

Figure 4.1: The comparison of sapphire with (a) measured values (b) standardized values

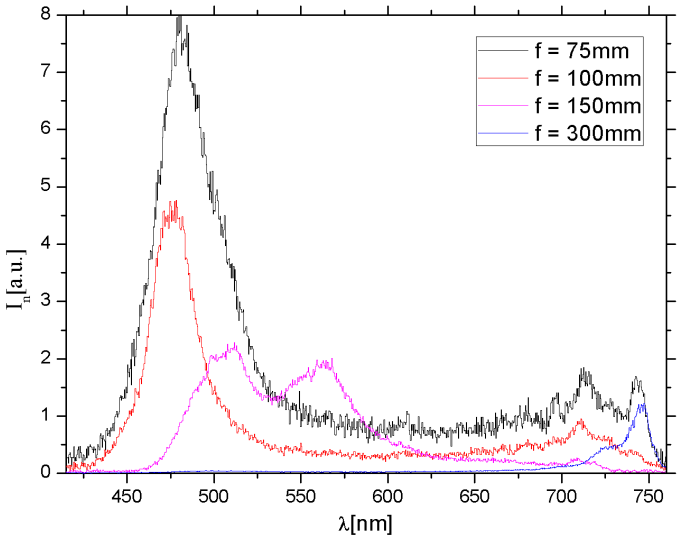

Figure 4.2: The comparison of sapphire with , cut-off = 395nm, cut-on = 765nm

$f = 75$mm, $z = 77$mm, $d = 2$mm, $P_1 = 21.10$mW, $P_2 = 1.56$mW, $\alpha = 254^o$, $l = 50$mm, cut-off = 410nm, cut-on = 755nm.

$f = 100$mm, $z = 104$mm, $d = 2.5$mm, $P_1 = 21.77$mW, $P_2 = 2.41$mW, $\alpha = 253^o$, $l = 53$mm, cut-off = 395nm, cut-on = 765nm.

$f = 150$mm, $z = 154$mm, $d = 5.5$mm, $P_1 = 4.75$mW, $P_2 = 2.91$mW, $\alpha = 242^o$, $l = 80$mm, cut-off = 450nm, cut-on = 730nm.

$f = 300$mm, $z = 310$mm, $d = 5.5$mm, $P_1 = 7.48$mW, $P_2 = 3.67$mW, $\alpha = 248^o$, $l = 70$mm, cut-off = 460nm, cut-on = 765nm.

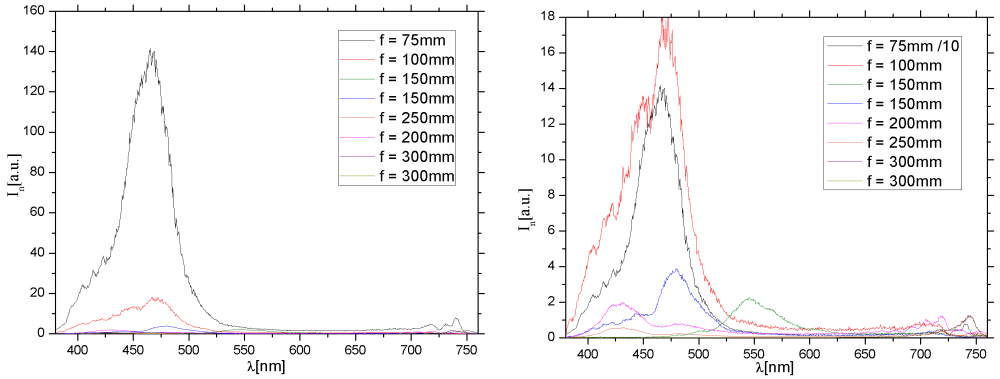

(a) (b)

Figure 4.3: The comparison of Quartz with cut-off = 430nm, cut-on = 770nm

(a) standardized values (b) standardized values of Quartz with f = 75mm divided by 10

$f = 75$mm, $z = 75$mm, $d = 2.0$mm, $P_1 = 20.32$mW, $P_2 = 2.10$mW, $\alpha = 289^o$, $l = 50$mm, cut-off = 385nm, cut-on = 755nm.

$f = 100$mm, $z = 100$mm, $d = 3.0$mm, $P_1 = 22.25$mW, $P_2 = 2.75$mW, $\alpha = 282^o$, $l = 57$mm, cut-off = 380nm, cut-on = 765nm.

$f = 150$mm, $z = 155$mm, $d = 5.5$mm, $P_1 = 5.19$mW, $P_2 = 3.39$mW, $\alpha = 185^o$, $l = 80$mm, cut-off = 450nm, cut-on = 735nm.

$f = 200$mm, $z = 200$mm, $d = 5.0$mm, $P_1 = 4.28$mW, $P_2 = 2.18$mW, $\alpha = 215^o$, $l = 64$mm, cut-off = 380nm, cut-on = 785nm.

$f = 250$mm, $z = 254$mm, $d = 4.0$mm, $P_1 = 10.73$mW, $P_2 = 4.68$mW, $\alpha = 215^o$, $l = 100$mm, cut-off = 380nm, cut-on = 730nm.

$f = 300$mm, $z = 318$mm, $d = 4.0$mm, $P_1 = 14.25$mW, $P_2 = 3.65$mW, $\alpha = 20^o$, $l = 45$mm, cut-off = 650nm, cut-on = 765nm.

$f = 300$mm, $z = 316$mm, $d = 4.0$mm, $P_1 = 7.51$mW, $P_2 = 3.90$mW, $\alpha = 20^o$, $l = 43$mm, cut-off = 430nm, cut-on = 770nm.

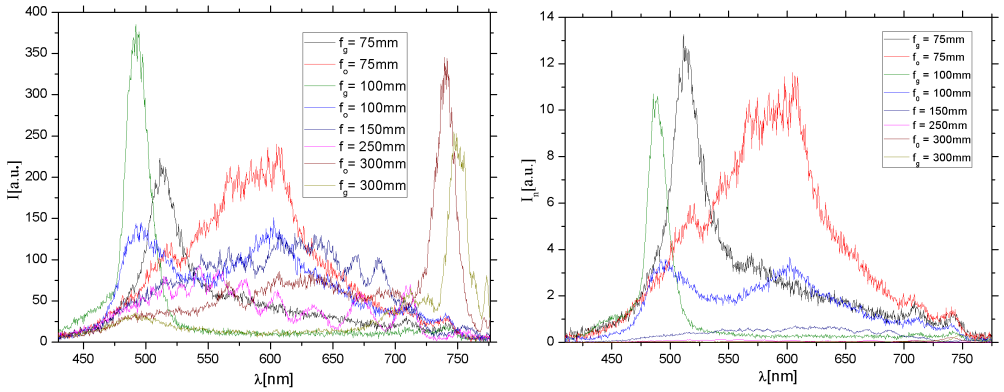

Figure 4.4: The comparison of YAP with cut-off = 400nm, cut-on = 770nm.
(a) measured values (b) standardized values

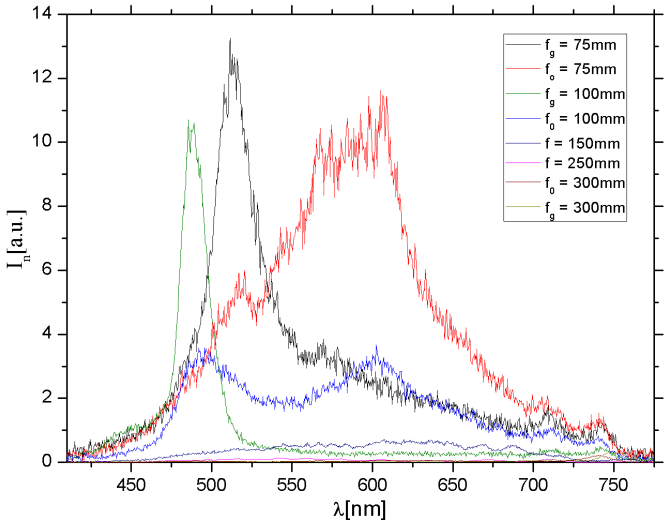

Figure 4.5: The comparison of YAP with cut-off = 400nm, cut-on = 770nm.

Y_g:f = 75mm, z = 75mm, d = 1.5mm, P_1 = 22.19mW, P_2 = 1.29mW, $\alpha = 223^o$, l = 55mm, cut-off= 400nm, cut-on= 755nm.

Y_o:f = 75mm, z = 78mm, d = 2.0mm, P_1 = 21.87mW, P_2 = 1.43mW, $\alpha = 223^o$, l = 52mm, cut-off= 400nm, cut-on= 755nm.

Y_g:f = 100mm, z = 102mm,d = 2.0mm,P_1 = 22.98mW,P_2 = 1.77mW,$\alpha = 223^o$, l = 53mm, cut-off= 420nm, cut-on= 755nm.

Y_o:f = 100mm ,z = 100mm,d = 2.0mm,P_1 = 22.52mW,P_2 = 1.75mW,$\alpha = 223^o$, l = 55mm, cut-off= 400nm, cut-on= 760nm.

Y:f = 150mm, z = 155mm, d = 5.5mm, P_1 = 5.12mW, P_2 = 3.24mW, $\alpha = 185^o$, l = 70mm, cut-off = 430nm, cut-on= 740nm.

Y:f = 250mm, z = 251mm,d = 3.5mm, P_1 = 10.80mW, P_2 = 3.71mW,$\alpha = 245^o$, l = 97mm, cut-off = 430nm, cut-on= 730nm.

Y_g:f = 300mm, z = 295mm, d = 3.0mm, P_1 = 14.46mW, P_2 = 3.98mW,$\alpha = 245^o$,l = 65mm, cut-off= 430nm, cut-on= 765nm.

Y_o:f = 300mm, z = 296mm, d = 4.0mm, P_1 = 7.45mW, P_2 = 3.85mW, $\alpha = 245^o$, l = 64mm, cut-off = 430nm, cut-on= 770nm.

4.1.2 The comparisons of crystals

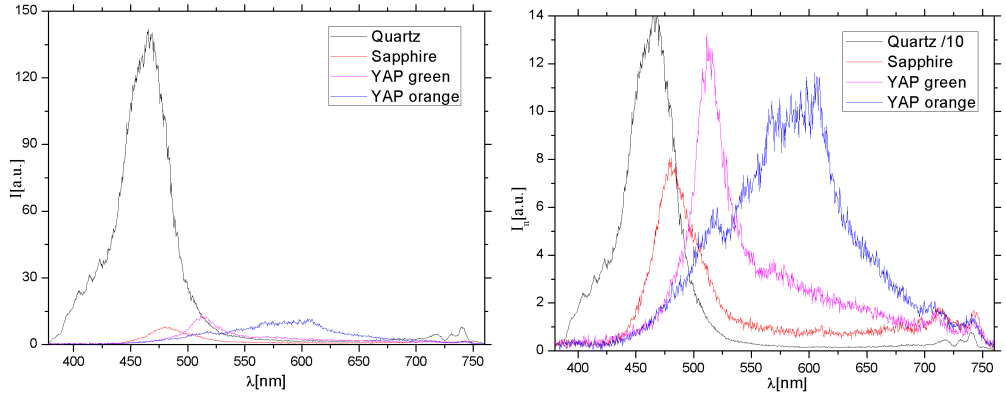

(a) (b)

Figure 4.6: The comparison of quartz, sapphire and YAP with with $f = 75$mm, cut-off = 385nm, cut-on = 755nm for (a) standardized values (b) standardized values and Quartz values divided by 10.
Q: $z = 75$mm, $d = 2$mm, $P_1 = 20.32$mW, $P_2 = 2.10$ mW, $\alpha = 289^o$, $l = 50$mm, cut-off = 385nm, cut-on = 755nm.
S: $z = 77$mm, $d = 2$mm, $P_1 = 21.10$mW, $P_2 = 1.56$mW, $\alpha = 254^o$, $l = 50$mm, cut-off = 410nm, cut-on = 755nm.
Y_g: $z = 75$mm, $d = 1.5$mm, $P_1 = 22.19$mW, $P_2 = 1.29$mW, $\alpha = 223^o$, $l = 55$mm, cut-off = 400nm, cut-on = 755nm.
Y_o: $z = 78$mm, $d = 2$mm, $P_1 = 21.87$mW, $P_2 = 1.43$mW, $\alpha = 223^o$, $l = 52$mm, cut-off = 400nm, cut-on = 755nm.

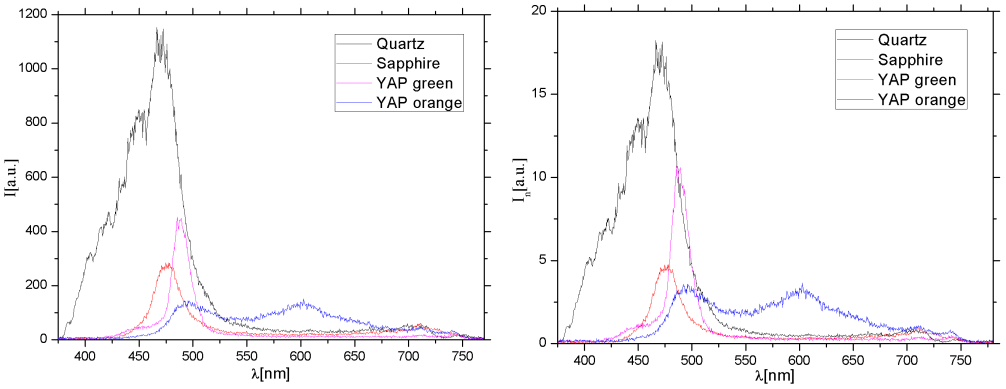

(a) (b)

Figure 4.7: The comparison of quartz, sapphire and YAP with with $f = 100$mm, cut-off = 380nm, cut-on = 765nm for (a) measured values (b) standardized values.

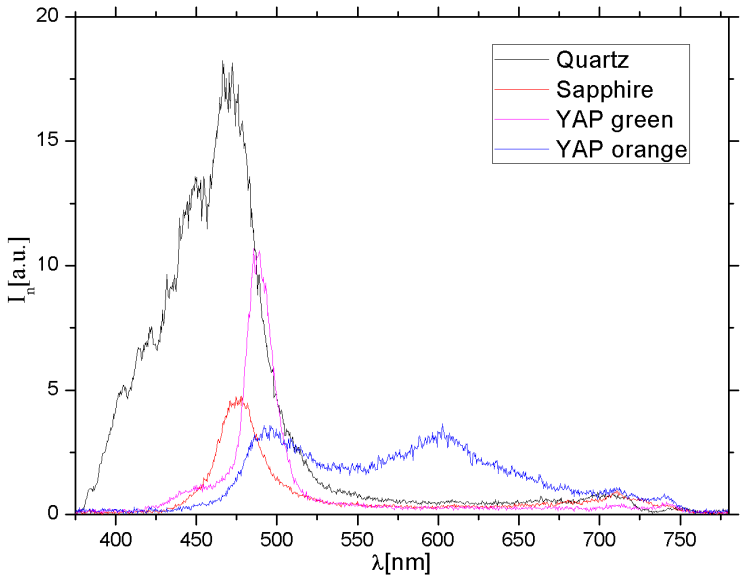

Figure 4.8: The comparison of quartz, sapphire and YAP with $f = 100$mm, cut-off = 380nm, cut-on = 765nm.
Q: $z = 100$mm, $d = 3$mm, $P_1 = 22.25$mW, $P_2 = 2.75$ mW, $\alpha = 282^o$, $l = 57$mm, cut-off = 380nm, cut-on = 765nm.
S: $z = 104$mm, $d = 2.5$mm, $P_1 = 21.77$mW, $P_2 = 2.41$mW, $\alpha = 253^o$, $l = 53$mm, cut-off = 395nm, cut-on = 765nm.
Y_g: $z = 102$mm, $d = 2.0$mm, $P_1 = 22.98$mW, $P_2 = 1.77$mW, $\alpha = 223^o$, $l = 53$mm, cut-off = 420nm, cut-on = 755nm.
Y_o: $z = 100$mm, $d = 2$mm, $P_1 = 22.52$mW, $P_2 = 1.75$mW, $\alpha = 223^o$, $l = 55$mm, cut-off = 400nm, cut-on = 760nm.

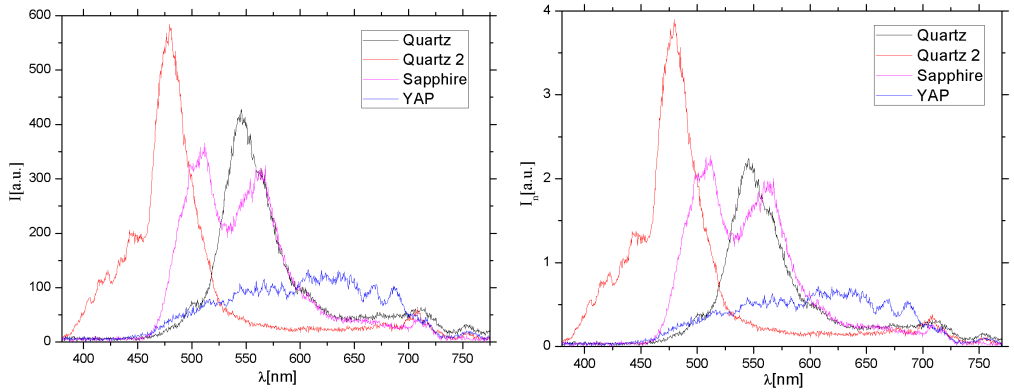

Figure 4.9: The comparison of quartz, sapphire and YAP with $f = 150$mm, cut-off = 380nm, cut-on = 740nm for (a) measured values (b) standardized values.

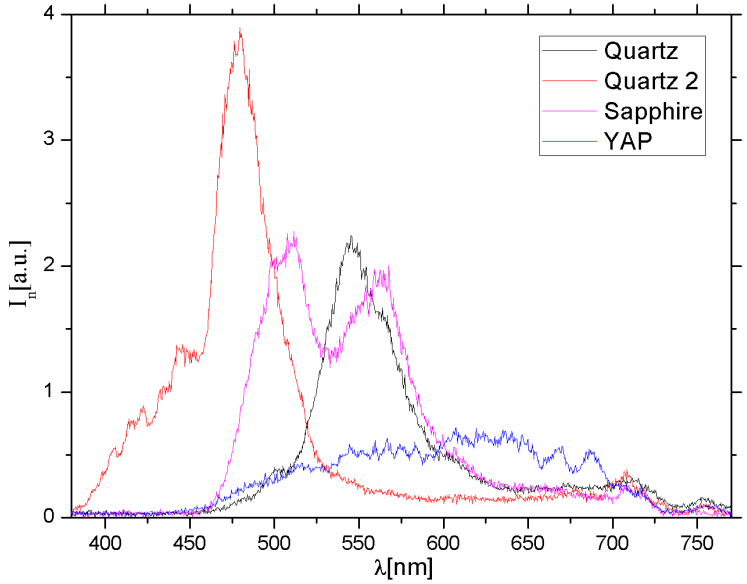

Figure 4.10: The comparison of quartz, sapphire and YAP with $f = 150$mm, cut-off = 380nm, cut-on = 740nm.
Q:$z = 155$mm, $d = 5.5$mm, $P_1 = 5.19$mW, $P_2 = 3.39$ mW, $\alpha = 185^o$, $l = 70$mm, cut-off = 450nm, cut-on = 735nm.
Q 2:$z = 150$mm, $d = 5.5$mm, $P_1 = 4.41$mW, $P_2 = 2.90$mW, $\alpha = 185^o$, $l = 55$mm, cut-off = 380nm, cut-on = 740nm.
S: $z = 154$mm, $d = 5.5$mm, $P_1 = 4.75$mW, $P_2 = 2.91$mW, $\alpha = 242^o$, $l = 80$mm, cut-off = 450nm, cut-on = 730nm.
Y: $z = 155$mm, $d = 5.5$mm, $P_1 = 5.12$mW, $P_2 = 3.24$mW, $\alpha = 185^o$, $l = 70$mm, cut-off = 430nm, cut-on = 740nm.

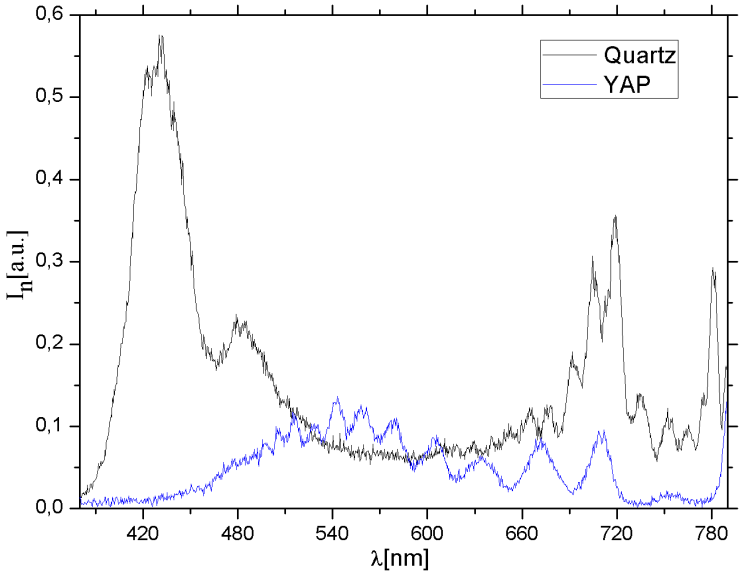

Figure 4.11: The comparison of quartz and YAP with $f = 250$mm, cut-off= 380nm, cut-on= 730nm.
Q: $z = 254$mm, $d = 4.0$mm, $P_1 = 10.73$mW, $P_2 = 4.68$mW, $\alpha = 215^o$, $l = 100$mm, cut-off= 380nm, cut-on= 730nm.
Y: $z = 251$mm, $d = 3.5$mm, $P_1 = 10.80$mW, $P_2 = 3.71$mW, $\alpha = 245^o$, $l = 97$mm, cut-off= 430nm, cut-on= 730nm.

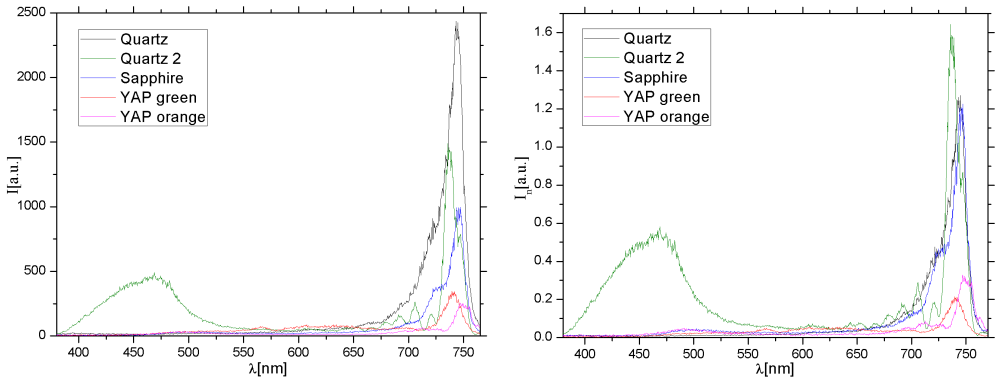

Figure 4.12: The comparison of quartz, sapphire and YAP with $f = 300$mm, cut-off= 380nm, cut-on= 765nm for (a) measured values (b) standardized values.

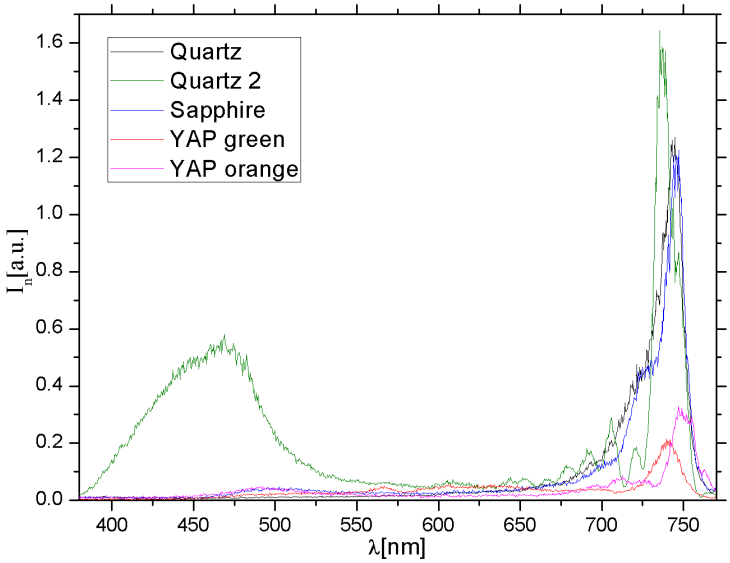

Figure 4.13: The comparison of quartz, sapphire and YAP with $f = 300$mm, cut-off= 380nm, cut-on= 765nm.
Q: $z = 318$mm, $d = 4.0$mm, $P_1 = 14.25$mW, $P_2 = 3.65$mW, $\alpha = 20^o$, $l = 45$mm, cut-off = 650nm, cut-on = 765nm.
Q 2: $z = 316$mm, $d = 4.0$mm, $P_1 = 7.51$mW, $P_2 = 3.90$mW, $\alpha = 20^o$, $l = 43$mm, cut-off = 380nm, cut-on = 760nm.
S: $z = 310$mm, $d = 5.5$mm, $P_1 = 7.48$mW, $P_2 = 3.67$mW, $\alpha = 248^o$, $l = 70$mm, cut-off = 460nm, cut-on = 765nm.
Y_g: $z = 295$mm,$d = 3.0$mm,$P_1 = 14.46$mW,$P_2 = 3.98$mW, $\alpha = 245^o$, $l = 65$mm, cut-off = 430nm, cut-on = 765nm.
Y_o: $z = 296$mm, $d = 4.0$mm, $P_1 = 7.45$mW, $P_2 = 3.85$mW, $\alpha = 245^o$, $l = 64$mm, cut-off = 430nm, cut-on = 765nm.

4.1.3 Angle dependence

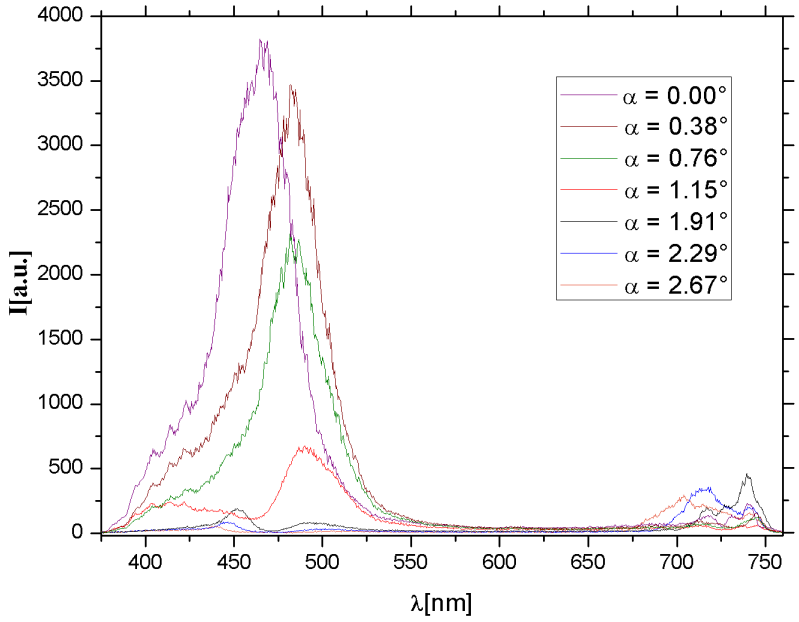

Figure 4.14: The comparison of quartz for various angles
Q: $z = 75$mm, $d = 2$mm, $P_1 = 20.32$mW, $P_2 = 2.10$ mW, $\alpha = 289^o$, $l = 50$mm, cut-off = 385nm, cut-on = 755nm.

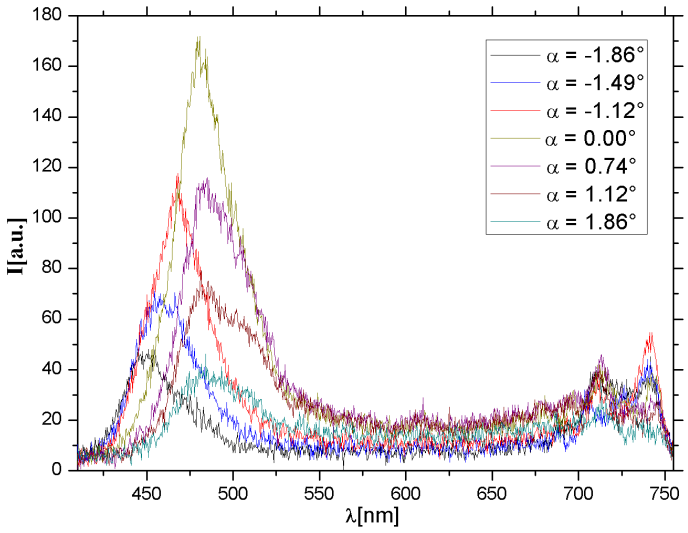

Figure 4.15: The comparison of sapphire for various angles
S: $z = 77$mm, $d = 2$mm, $P_1 = 21.10$mW, $P_2 = 1.56$mW, $\alpha = 254^o$, $l = 50$mm, cut-off = 410nm, cut-on = 755nm.

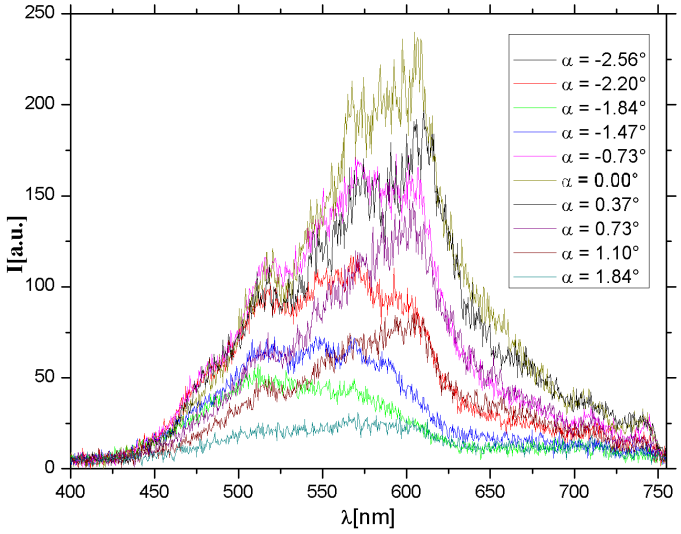

Figure 4.16: The comparison of YAP orange for various angles
Y_o: $z = 78$mm, $d = 2$mm, $P_1 = 21.87$mW, $P_2 = 1.43$mW, $\alpha = 223^o$, $l = 52$mm, cut-off = 400nm, cut-on = 755nm.

4.2 Infrared region

4.2.1 Spectra of Quartz, Sapphire and YAP for Various Focal Lengths

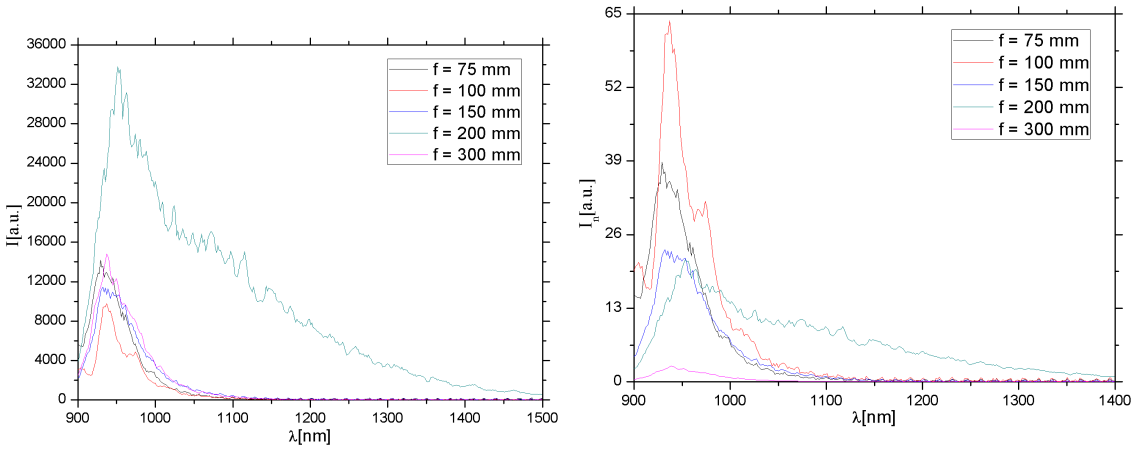

(a) (b)

Figure 4.17: The comparison of quartz with cut-off = 900nm, cut-on = 1460nm for
(a) measured values (b) standardized values.
$f = 75$mm, $z = 78$mm, $d = 3.0$mm, $P_1 = 21.38$mW, $P_2 = 3.21$ mW, $\alpha = 290^o$, $l = 59$mm, cut-off = 900nm, cut-on = 1050nm.
$f = 100$mm, $z = 100$mm, $d = 3.0$mm, $P_1 = 22.11$mW, $P_2 = 2.46$mW, $\alpha = 282^o$, $l = 55$mm, cut-off= 900nm, cut-on= 1060nm.
$f = 150$mm, $z = 152$mm, $d = 3.0$mm, $P_1 = 21.45$mW, $P_2 = 3.40$mW, $\alpha = 267^o$, $l = 59$mm, cut-off= 900nm, cut-on= 1100nm.
$f = 200$mm, $z = 198$mm, $d = 4.0$mm, $P_1 = 4.58$mW, $P_2 = 2.20$mW, $\alpha = 215^o$, $l = 75$mm, cut-off= 900nm, cut-on= 1460nm.
$f = 300$mm, $z = 290$mm, $d = 5.0$mm, $P_1 = 7.31$mW, $P_2 = 3.49$mW, $\alpha = 20^o$, $l = 71$mm, cut-off= 900nm, cut-on= 1150nm.

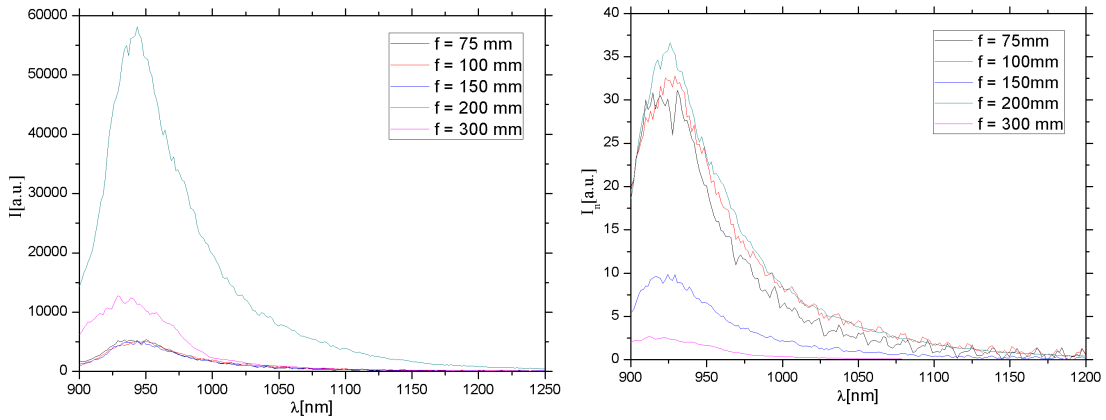

(a) (b)

Figure 4.18: The comparison of sapphire with cut-off = 900nm, cut-on = 1460nm for (a) measured values (b) standardized values.

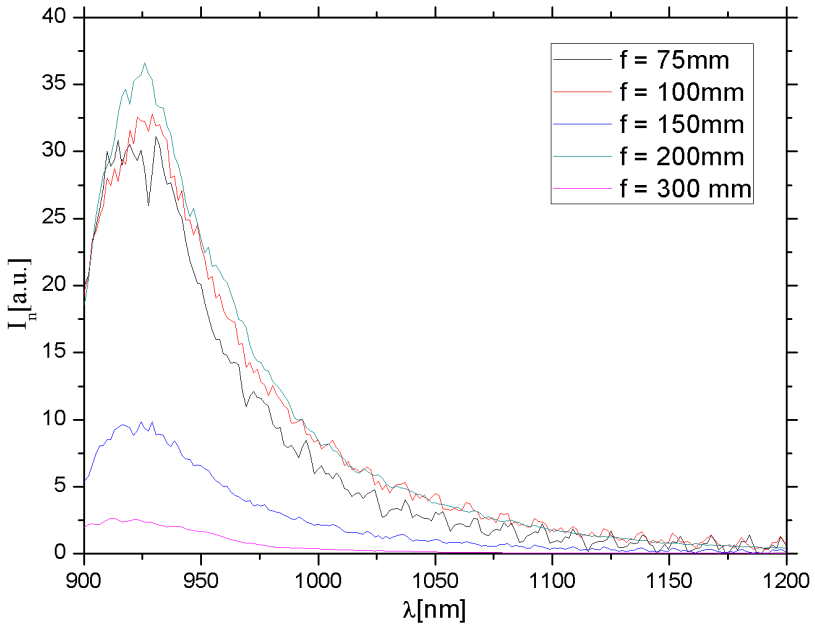

Figure 4.19: The comparison of sapphire with cut-off = 900nm, cut-on = 1170nm.
$f = 75$mm, $z = 77$mm, $d = 2.0$mm, $P_1 = 21.63$mW, $P_2 = 1.56$mW, $\alpha = 252^o$, $l = 60$mm, cut-off= 900nm, cut-on= 1100nm.
$f = 100$mm, $z = 100$mm, $d = 2.5$mm, $P_1 = 21.62$mW, $P_2 = 2.51$mW, $\alpha = 252^o$, $l = 52$mm, cut-off= 900nm, cut-on= 1130nm.
$f = 150$mm, $z = 153$mm, $d = 3.0$mm, $P_1 = 19.19$mW, $P_2 = 3.52$mW, $\alpha = 252^o$, $l = 75$mm, cut-off= 900nm, cut-on= 1120nm.
$f = 200$mm, $z = 197$mm, $d = 4.0$mm, $P_1 = 4.60$mW, $P_2 = 2.25$mW, $\alpha = 248^o$, $l = 74$mm, cut-off= 900nm, cut-on= 1170nm.
$f = 300$mm, $z = 289$mm, $d = 5.5$mm, $P_1 = 7.58$mW, $P_2 = 3.17$mW, $\alpha = 248^o$, $l = 70$mm, cut-off= 900nm, cut-on= 1070nm.

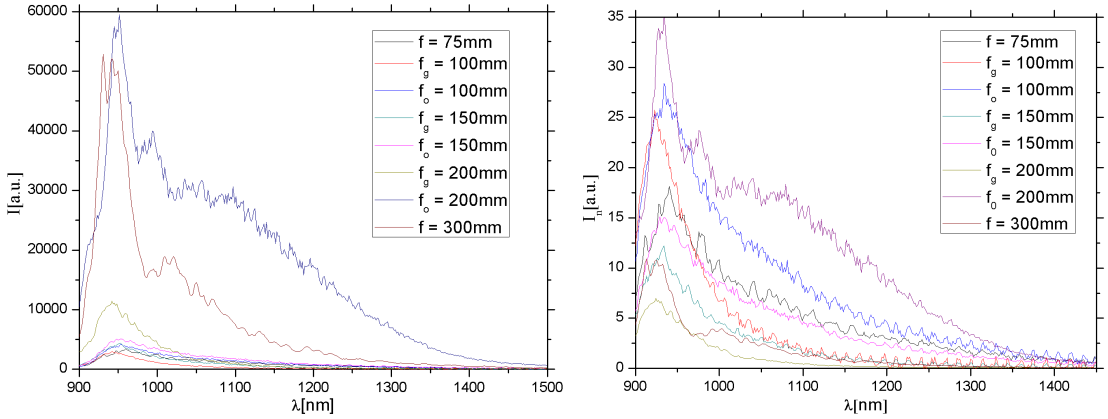

(a) (b)

Figure 4.20: The comparison of YAPwith cut-off = 900nm, cut-on = 1450nm for (a) measured values (b) standardized values.

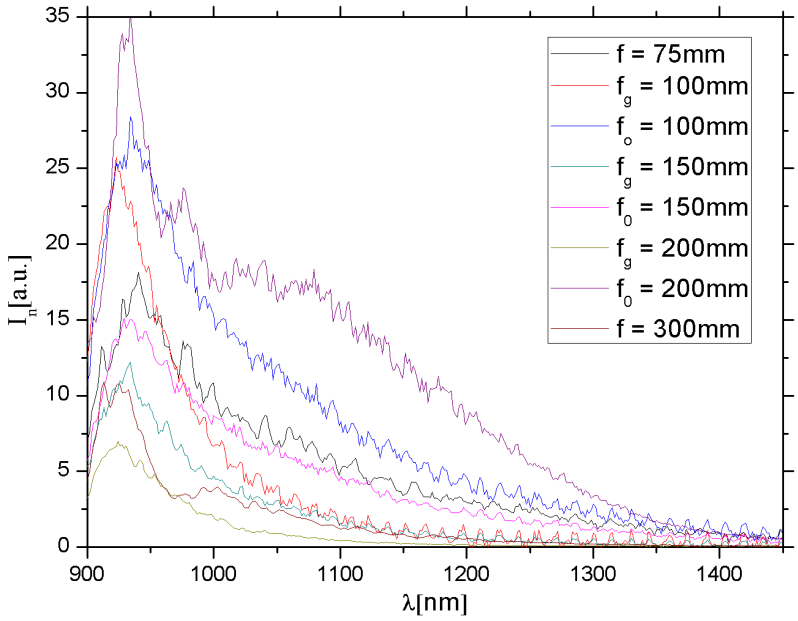

Figure 4.21: The comparison of YAP with cut-off = 900nm, cut-on = 1450nm.
Y: $f = 75$mm, $z = 79$mm, $d = 2.0$, $P_1 = 22.09$mW, $P_2 = 1.60$mW, $\alpha = 223^o$, $l = 60$mm, cut-off= 900nm, cut-on= 1400nm.
Y_g:$f = 100$mm,$z = 102$mm,$d = 2.5$mm,$P_1 = 16.81$mW,$P_2 = 1.78$mW,$\alpha = 223^o$,$l = 50$mm, cut-off= 900nm, cut-on= 1120nm.
Y_o:$f = 100$mm,$z = 100$mm,$d = 2.0$mm,$P_1 = 16.97$mW,$P_2 = 2.36$mW,$\alpha = 223^o$, $l = 52$mm, cut-off= 900nm, cut-on= 1400nm.
Y_g:$f = 150$mm,$z = 147$mm,$d = 3.0$mm,$P_1 = 20.87$mW,$P_2 = 2.69$mW,$\alpha = 223^o$,$l = 66$mm, cut-off= 900nm, cut-on= 1250nm.
Y_o:$f = 150$mm, $z = 152$mm, $d = 3.0$mm,$P_1 = 19.20$mW,$P_2 = 2.34$mW,$\alpha = 223^o$, $l = 61$mm, cut-off= 900nm, cut-on= 1400nm.
Y_g:$f = 200$mm ,$z = 202$mm, $d = 4.0$mm,$P_1 = 4.53$mW,$P_2 = 2.21$mW,$\alpha = 236^o$, $l = 69$mm, cut-off= 900nm, cut-on= 1200nm.
Y_o:$f = 200$mm, $z = 206$mm, $d = 5.0$mm,$P_1 = 4.50$mW,$P_2 = 2.20$mW,$\alpha = 210^o$, $l = 80$mm, cut-off= 900nm, cut-on= 1450nm.
Y:$f = 300$mm, $z = 290$mm, $d = 4.0$mm, $P_1 = 7.20$mW, $P_2 = 3.16$mW, $\alpha = 245^o$, $l = 71$mm, cut-off= 900nm, cut-on= 1250nm.

4.2.2 The comparisons of crystals

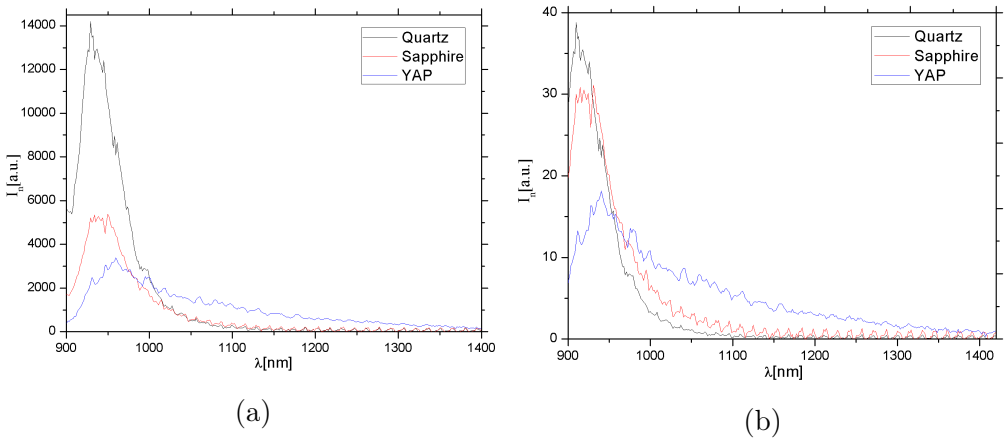

Figure 4.22: The comparison of quartz, sapphire and YAP with $f = 75$mm, cut-off = 900nm, cut-on = 1430nm for (a) measured values (b) standardized values.

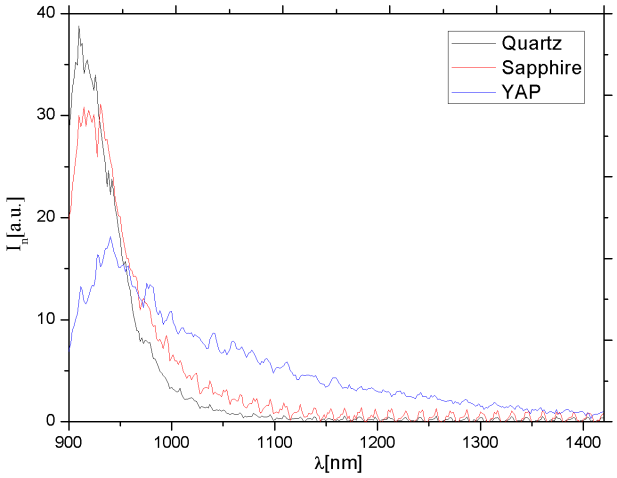

Figure 4.23: The comparison of quartz, sapphire and YAP with $f = 75$mm, cut-off = 900nm, cut-on = 1430nm. Quartz: $z = 78$mm, $d = 3.0$mm, $P_1 = 21.38$mW,$P_2 = 3.21$ mW, $\alpha = 290^o$, $l = 59$mm, cut-off = 900nm, cut-on = 1050nm. Sapphire: $z = 77$mm, $d = 2.0$mm, $P_1 = 21.63$mW,$P_2 = 1.56$mW,$\alpha = 252^o$, $l = 60$mm, cut-off = 900nm, cut-on = 1100nm. YAP: $z = 79$mm, $d = 2.0$mm, $P_1 = 22.09$mW, $P_2 = 1.60$mW, $\alpha = 223^o$, $l = 60$mm, cut-off = 900nm, cut-on = 1430nm.

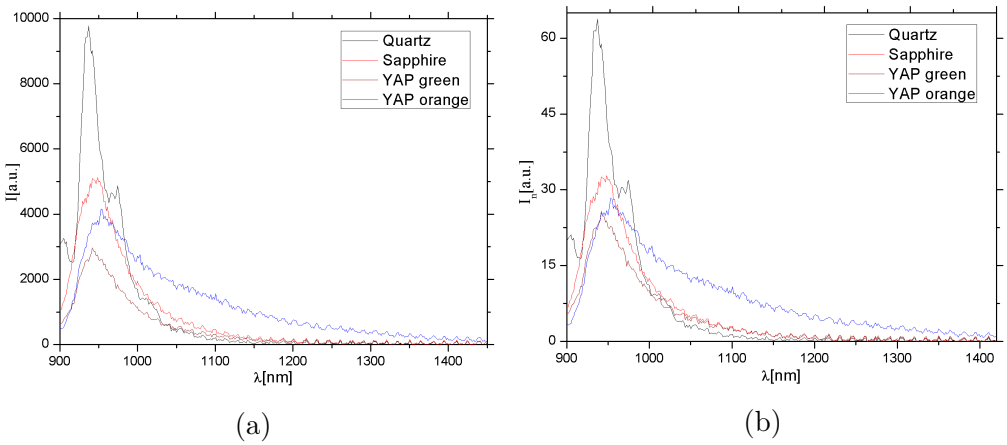

Figure 4.24: TThe comparison of quartz, sapphire and YAP with $f = 100$mm, cut-off = 900nm, cut-on = 1430nm for (a) measured values (b) standardized values.

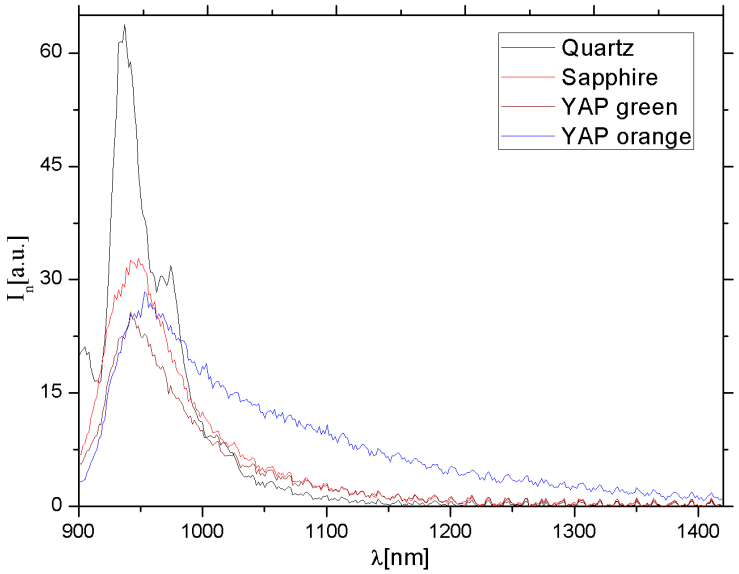

Figure 4.25: The comparison of quartz, sapphire and YAP with $f = 100$mm, cut-off = 900nm, cut-on = 1430nm. Q: $z = 100$mm, $d = 3.0$mm, $P_1 = 22.11$mW, $P_2 = 2.46$ mW, $\alpha = 282^o$, $l = 55$mm, cut-off = 900nm, cut-on = 1060nm. S: $z = 100$mm, $d = 2.5$mm, $P_1 = 21.62$mW, $P_2 = 2.51$mW, $\alpha = 252^o$, $l = 52$mm, cut-off = 900nm, cut-on = 1130nm. Y_g: $z = 102$mm, $d = 2.5$mm, $P_1 = 16.81$mW, $P_2 = 1.78$mW, $\alpha = 223^o$, $l = 50$mm, cut-off = 900nm, cut-on = 1120nm. Y_o: $z = 100$mm, $d = 2.0$mm, $P_1 = 16.97$mW, $P_2 = 2.36$mW, $\alpha = 223^o$, $l = 52$mm, cut-off = 900nm, cut-on = 1430nm.

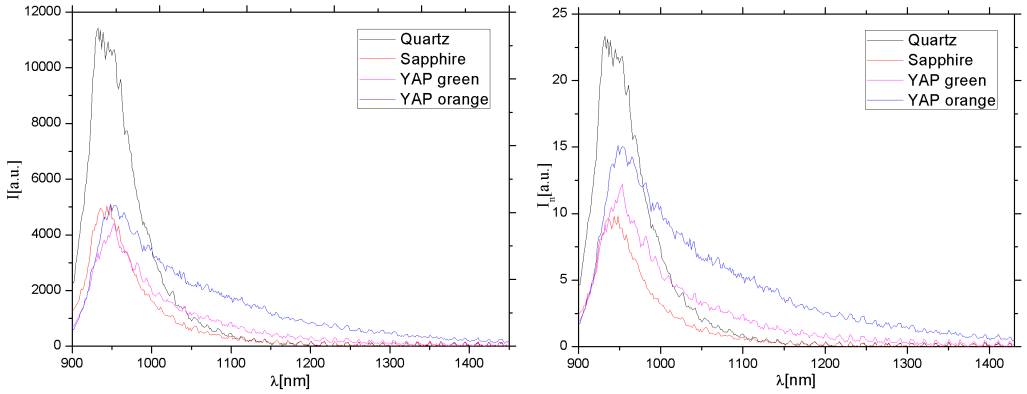

Figure 4.26: TThe comparison of quartz, sapphire and YAP with $f = 150$mm, cut-off = 900nm, cut-on = 1440nm for (a) measured values (b) standardized values.

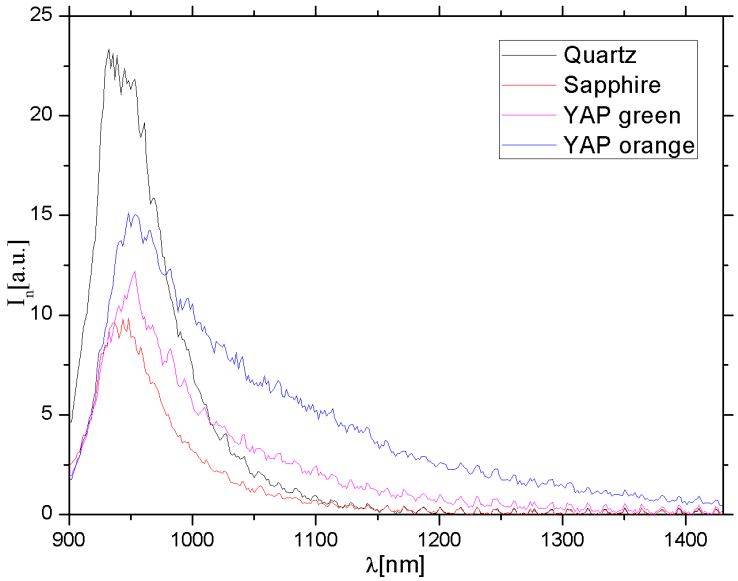

Figure 4.27: The comparison of quartz, sapphire and YAP with $f = 150$mm, cut-off = 900nm, cut-on = 1440nm.
Q: $z = 152$mm, $d = 3.0$mm, $P_1 = 21.45$mW, $P_2 = 3.40$ mW, $\alpha = 267^o$, $l = 59$mm, cut-off = 900nm, cut-on = 1100nm.
S: $z = 153$mm, $d = 3.0$mm, $P_1 = 19.19$mW, $P_2 = 3.52$mW, $\alpha = 252^o$, $l = 75$mm, cut-off = 900nm, cut-on = 1120nm.
Y_g: $z = 147$mm, $d = 3.0$mm, $P_1 = 20.87$mW, $P_2 = 2.69$mW, $\alpha = 223^o$, $l = 66$mm, cut-off = 900nm, cut-on = 1250nm.
Y_o: $z = 152$mm, $d = 3.0$mm, $P_1 = 19.20$mW, $P_2 = 2.34$mW, $\alpha = 223^o$, $l = 61$mm, cut-off = 900nm, cut-on = 1440nm.

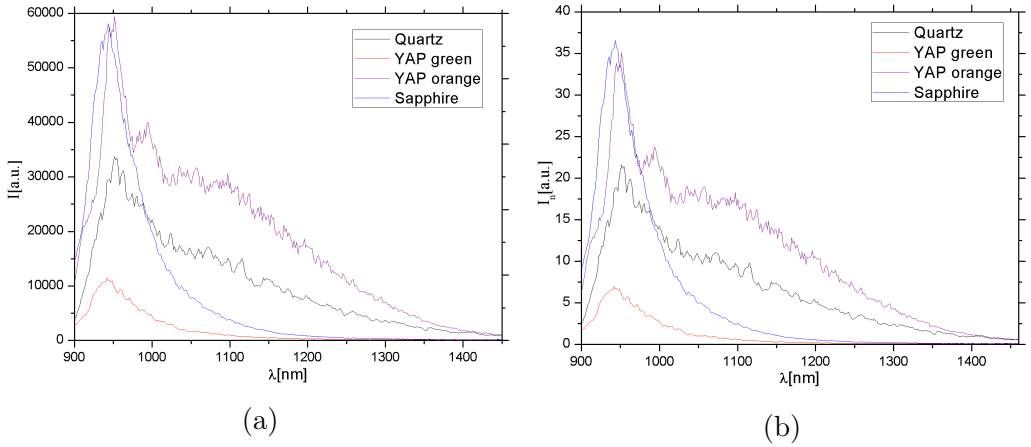

Figure 4.28: The comparison of quartz, sapphire and YAP with $f = 200$mm, cut-off = 900nm, cut-on = 1460nm for (a) measured values (b) standardized values.

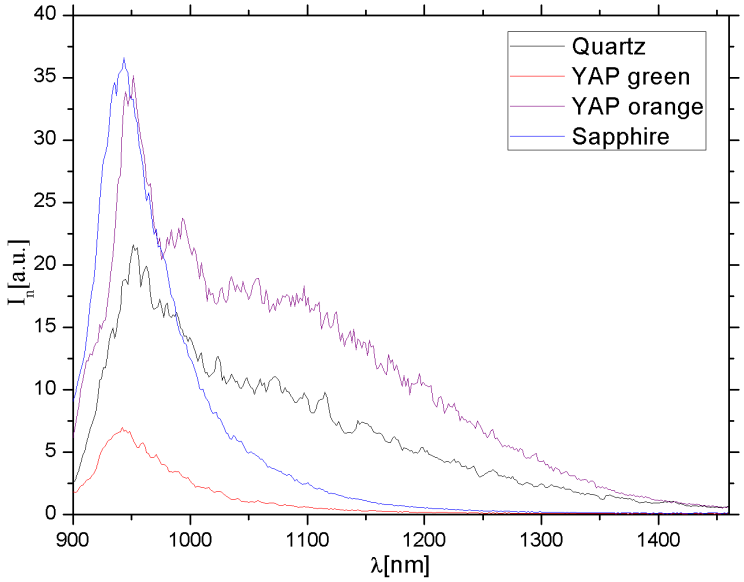

Figure 4.29: The comparison of quartz, sapphire and YAP with $f = 200$mm, cut-off = 900nm, cut-on = 1460nm.
Q: $z = 198$mm, $d = 4.0$mm, $P_1 = 4.58$mW, $P_2 = 2.20$ mW, $\alpha = 215^o$, $l = 75$mm, cut-off = 900nm, cut-on = 1460nm.
Y_g: $z = 202$mm, $d = 4.0$mm, $P_1 = 4.53$mW, $P_2 = 2.21$mW, $\alpha = 236^o$, $l = 69$mm, cut-off = 900nm, cut-on = 1200nm.
Y_o: $z = 206$mm, $d = 5.0$mm, $P_1 = 4.50$mW, $P_2 = 2.20$mW, $\alpha = 210^o$, $l = 80$mm, cut-off = 900nm, cut-on = 1450nm.
S: $z = 197$mm, $d = 4.0$mm, $P_1 = 4.60$mW, $P_2 = 2.25$mW, $\alpha = 248^o$, $l = 74$mm, cut-off = 900nm, cut-on = 1170nm.

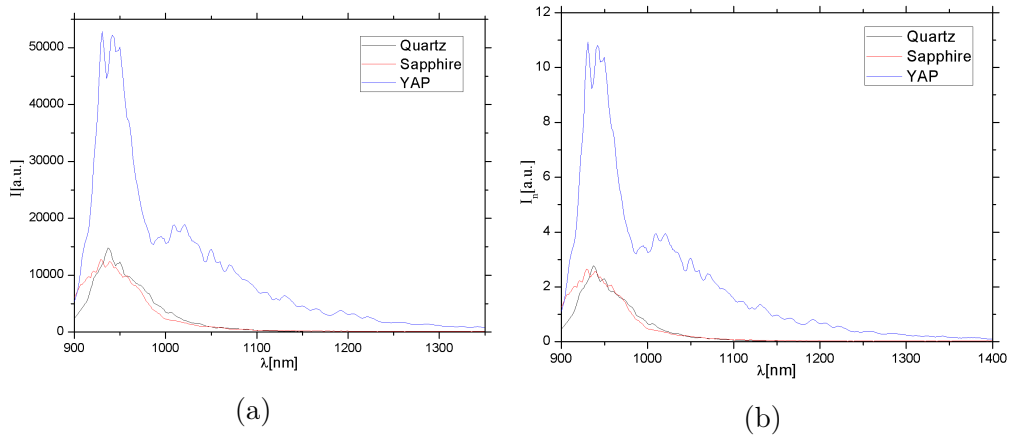

Figure 4.30: The comparison of quartz, sapphire and YAP with $f = 300$mm, cut-off = 900nm, cut-on = 1400nm for (a) measured values (b) standardized values.

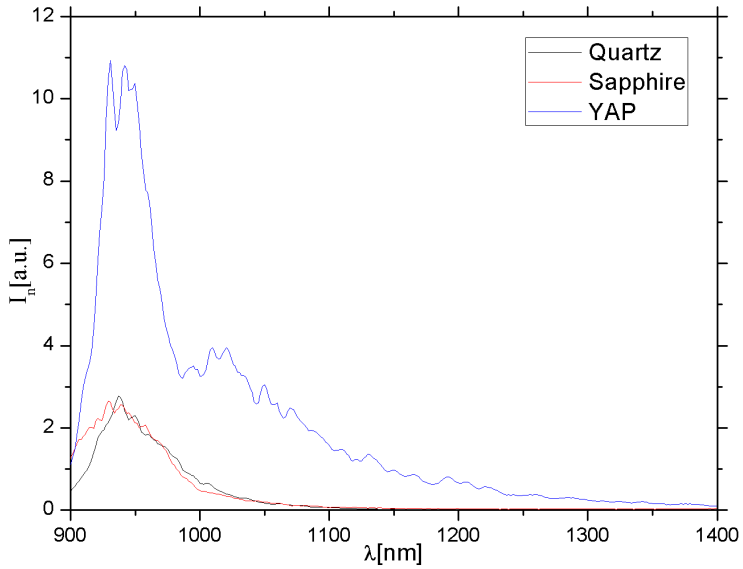

Figure 4.31: The comparison of quartz, sapphire and YAP with $f = 300$mm, cut-off = 900nm, cut-on = 1400nm.
Q: $z = 290$mm, $d = 5.0$mm, $P_1 = 7.31$mW, $P_2 = 3.49$ mW, $\alpha = 20^o$, $l = 71$mm, cut-off = 900nm, cut-on = 1150nm.
S: $z = 289$mm, $d = 5.5$mm, $P_1 = 7.58$mW, $P_2 = 3.17$mW, $\alpha = 248^o$, $l = 70$mm, cut-off = 900nm, cut-on = 1070nm.
Y: $z = 290$mm, $d = 4.0$mm, $P_1 = 7.20$mW, $P_2 = 3.16$mW, $\alpha = 245^o$, $l = 71$mm, cut-off = 900nm, cut-on = 1250nm.

4.2.3 Angle dependence

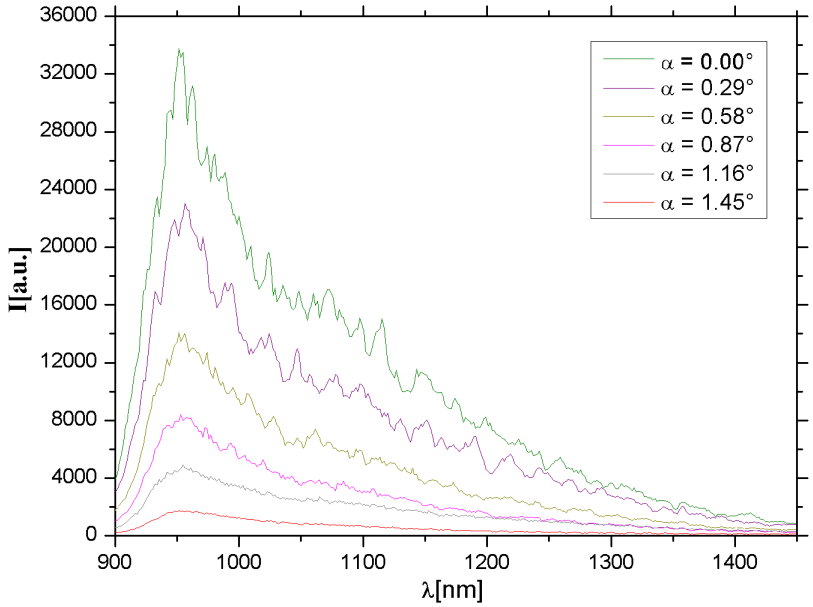

Figure 4.32: The comparison of quartz for various angles
Q: $z = 198$mm, $d = 4.0$mm, $P_1 = 4.58$mW, $P_2 = 2.20$ mW, $\alpha = 215^o$, $l = 75$mm, cut-off = 900nm, cut-on = 1460nm.

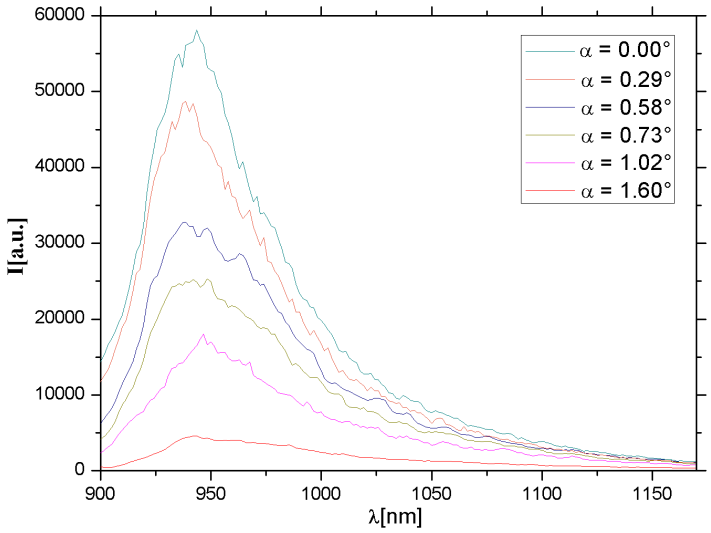

Figure 4.33: The comparison of sapphire for various angles
S: $z = 197$mm, $d = 4.0$mm, $P_1 = 4.60$mW, $P_2 = 2.25$mW, $\alpha = 248^o$, $l = 74$mm, cut-off = 900nm, cut-on = 1170nm.

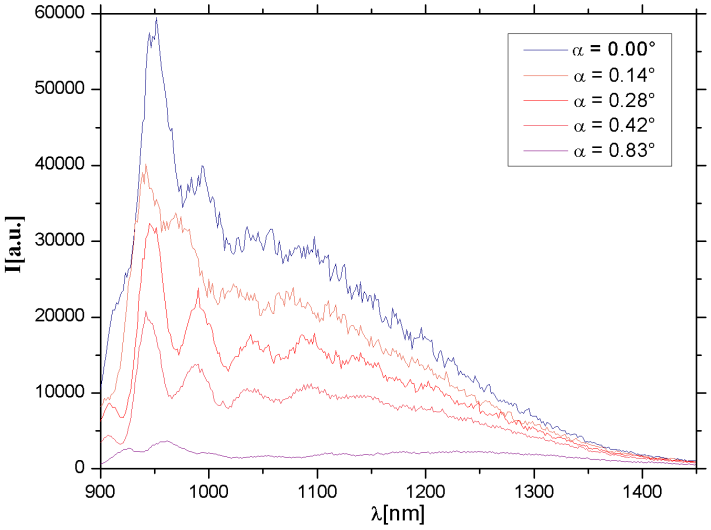

Figure 4.34: The comparison of YAP orange for various angles
Y_o: $z = 206$mm, $d = 5.0$mm, $P_1 = 4.50$mW, $P_2 = 2.20$mW, $\alpha = 210^o$, $l = 80$mm, cut-off = 900nm, cut-on = 1450nm.

4.3 Examples of wrongly generated spectra

In this section, the graphs with wrong parameters are shown. For example, when a high power beam passes through the crystal, then some oscillations emerge in the profile of its white light spectrum. There was an effort to generate single filament white light, where these ocsillations do not appear. This is shown in Figure 4.35. Different situation is pictured in Figure 4.36. There are some parameters for which the white light continuum is not generated.

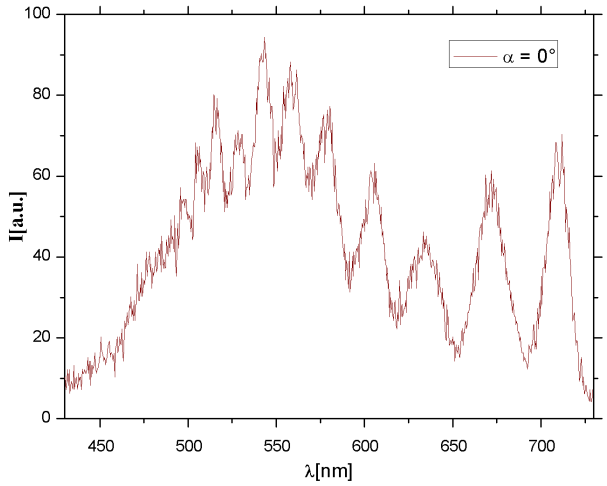

Figure 4.35: Oscillations in spectra with too much input power P_2
Y: $z = 251$mm, $d = 5.5$mm, $P_1 = 10.80$mW, $P_2 = 4.71$mW, $\alpha = 245^o$, $l = 97$mm, cut-off = 430nm, cut-on = 730nm.

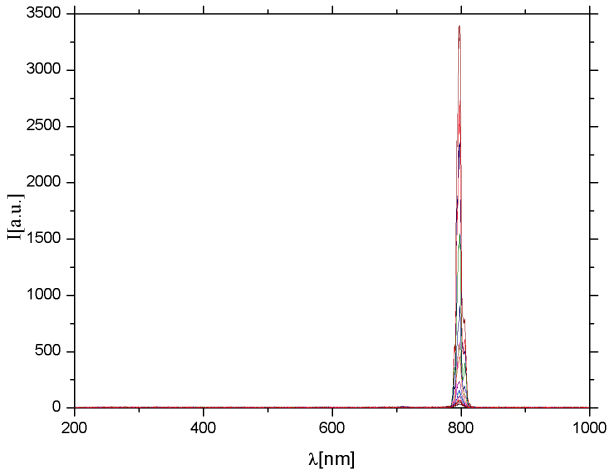

Figure 4.36: No spectral broadening
S: $z = 254$mm, $d = 5.5$mm, $P_1 = 10.67$mW, $P_2 = 4.60$mW, $\alpha = 238^o$, $l = 100$mm

5 Results and Discussion

The supercontinuum spectra depend on the various parameters, e.g. the diameter of the iris aperture d, the power P_2 [1] or the focal length of the used converging lens f. All parameters can be found below the figures of measured spectra in Chapter 4. There, we can see four various comparisons of the white light spectra of the three plates (quartz, sapphire and YAP).

At first sight, the order of quality of supercontinuum spectra differs from that with standardized spectra as can be seen in Figure 4.1. For final conclusions the relation of the standardized light intensity (Eq.3.2) was used and with its help, the first comparison of suprecontinuum spectra was made. For example, in Figure 4.1, part (a), the highest intensity was measured for sapphire with $f = 300$ mm, on the other hand, in part (b), where standardized spectra are presented, it is $f = 75$ mm with the highest intensity and the best spectral broadening. The overall result of this comparison is that the plate with the best behaviour for the white light generation in the visible region for various focal lengths is quartz. This statement is confirmed by values in the Table 5.1. In it the calculated areas of spectrum intensity under the curve are there. This method of computation has been described in Section 3.1.

The table 5.1 contains six columns: the focal lengths and the names of used plates. The last three columns belong to YAP. When we were successful, two kinds of the white light spectra were generated in YAP. These values are in the fourth and fifth column. There is no need of the sixth column. However, for some focal lengths, only one spectrum was generated in YAP, and its value is written in the sixth column. In this case, two previous columns in the same row are not used.

For sapphire with $f = 250$ mm, the value of spectral area is missing. No white light was generated (see Fig. 4.36). It may be caused by the high power passing through the plate. As we can see from the values below the figure, its power magnitude is twice the size than in other cases. In Fig. 4.35, the same mistake is shown for the YAP spectrum. In this case the large amount of energy caused the oscillations in its spectral profile.

From the table 5.1 and all comparison graphs in the visible region in Chapter 4, we can conclude that the most prominent spectral broadening was generated by use of the lens with $f = 75$mm. On the other hand, the worst white light continuum was generated for the lens with $f = 300$ mm. So, we may say that, in the visible region, with increasing focal length

[1] the power measured behind the aperture

the quality of the generated white light continuum decreases.

Table 5.1: Calculated values of the white light spectra intensity in the visible region

f[mm]	I_Q[a.u.]	I_S[a.u.]	I_{Yg}[a.u.]	I_{Yo}[a.u.]	I_Y[a.u.]
75	18724.19	1390.93	2177.72	3293.60	X
100	2915.13	642.91	820.79	1279.75	X
150	566.91	513.15	X	X	268.04
250	509.97	X	X	X	49.00
300	191.81	90.04	31.67	35.02	X

The same methods were applied in the infrared region, but they led to different results. The spectra in Section 4.2 show that YAP is the crystal with the best spectral broadening. The values in the table 5.2 confirm this result and add the best focal length $f = 200$ mm. Unfortunately, there is no apparent relation between the focal length and the quality of the white light spectra in NIR spectral region in our experiment.

Another important thing in the comparison of the white light generation in crystals is the temporal stability. Not all spectra were stable in time. If we use sapphire for supercontinuum generation, its spectra are stable in time. Quartz has the similar property. On the other hand, the spectral broadening caused by YAP is unstable and after a short time it disappears. The reason of its behaviour may be in a heat dissipation abilty of the crystals. The resulting supercontinuum is the combination of several nonlinear effects, it is therefore highly sensitive of the laser beam parameters and the nonlinear media. When the laser beam passes through a medium, this medium gets warmer and the structure of YAP may be more sensitive than other crystal structures. So, when the YAP was used, it was neccessery to put a barrier in front of the crystal plate to stop the laser beam in passing through it, or move with the plate before every measurement.

Table 5.2: Calculated values of the white light spectra intensity in the infrared region

f[mm]	I_Q[a.u.]	I_S[a.u.]	I_{Yg}[a.u.]	I_{Yo}[a.u.]	I_Y[a.u.]
75	1479.66	1533.75	X	X	1775.94
100	2200.30	1736.35	1338.75	2745.78	X
150	1104.68	495.26	790.60	1493.32	X
200	2287.39	1877.98	3836.49	3853.00	X
300	115.11	123.04	X	X	628.18

Supercontinuum generated in sapphire is shown in Fig. 5.1. We can see colored concentric circles caused by the four-wave mixing, self-phase modulation and self-steeping effects and

by satisfying the phase-matching condition (see Eq. 2.9) for the corresponding wavelength (see Section 2.1) [9]. The colors move outward from red to blue. The spectral profile of concentric circles is shown in Fig. 4.15. There is an angular dependence of the white light. We can see that intensity peaks move by the changes of the angle to the left (blueshift) or to the right (redshift).

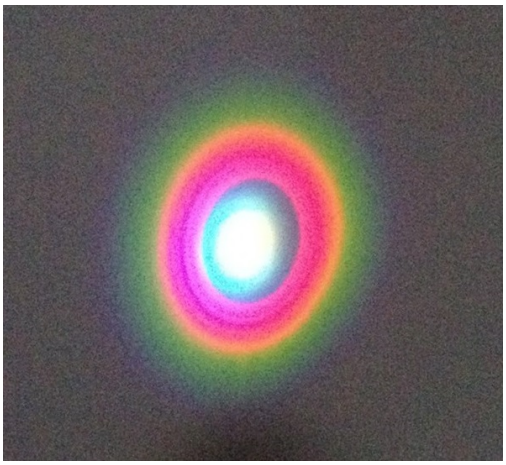

Figure 5.1: Supercontinuum generated by sapphire plate

6 Conclusions

The main aim of this thesis was to find the best configuration for the white light generation in the UV, visible and the near IR spectral region. The energy of the input pulse, the iris aperture diameter, the focal length of the converging lens and the crystal plates (YAP, quartz and sapphire) were changed to reach the best spectral broadening. In the end, the UV spectral region was not studied. The CaF_2 crystal plate was not measured due to the lack of time.

The most suitable crystal plate for supercontinuum generation in the visible region is quartz with focal lenght $f = 75$ mm. If we want to generate supercontinuum in sapphire or YAP, we should use lens with $f = 75$ mm to reach the best spectral broadening. In this experiment, the quality of the white light continuum decreases with increasing focal length.

Another situation occurs in the infrared region. There, the best focal length for all crystal plates for supercontinuum generation is $f = 200$ mm. In the comparison of crystals with this focal length, the most significant crystal was YAP. However, its spectra were unstable. When the YAP was used for supercontinuum generation, we had to move with it or put the barrier in front of it to stop the laser beam in passing through this crystal plate. If we do not want to take care of the spectrum stability, the next in order is quartz. In this region, nothing could be said about the dependence between the quality of the supercontinuum spectra and the focal length.

References

[1] R. W. Boyd: *Nonlinear optics - Third Edition*. Elsevier, Inc. London, 2008. ISBN: 978-0-12-369470-b.

[2] F. Zernike, J. E. Midwinter: *Applied Nonlinear Optics*. Dover Publications, Inc. Mineola, New York, 1973. ISBN-13: 978-0-486-45360-6.

[3] M.Vrbová a kol.: *Oborová encyklopedie - Lasery a moderní optika*. Prometheus. Praha, 1994. ISBN: 80-85849-56-9.

[4] B. E. A. Saleh, M. C. Teich: *Fundamentals of Photonics - Second Edition*. John Wiley and Son, Hoboken. USA, 2007. ISBN: 978-0-471-35832-9.

[5] Václav Sochor: *Lasery a koherentní svazky*. Academia. Praha, 1990. ISBN: 80-200-354-1.

[6] Petr Malý: *Optika*. Karolinum. Praha, 2008. ISBN: 978-80-246-1342-0.

[7] Frank Trager(Ed.): *Handbook of lasers and optics - Second Edition*. Springer. Germany, 2012. ISBN: 978-3-642-19408-5.

[8] R.R. Alfano, S.L. Shapiro: *Emission in the region 4000 to 7000 angstrom via four-photon coupling in glass*. 1970.

[9] R. W. Boyd,S. G. Lukishova, Y. R. Shen (Ed.): *Self-focusing: Past and the Present, Fundamentals and Prospects*. Springer, 2009. ISBN 978-0-387-34727-1.

[10] Fischer, Heinrich, Maier, Jungwirth, Brida and Leitenstorfer: *615 fs pulses with 17 mJ energy generated by an Yb:thin-disk amplifier at 3 kHz repetition rate*. Germany, 2016